



**LIBRARY**  
**Michigan State**  
**University**

This is to certify that the

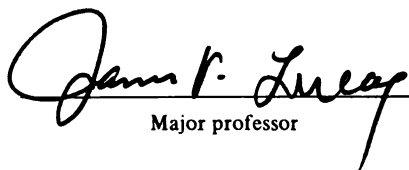
thesis entitled  
HYDROGEN CHARGING AND THE EFFECT OF CATHODIC  
CHARGED HYDROGEN IN A  
PARTICULATE - REINFORCED ALUMINUM COMPOSITES

presented by

Chidambara Ramalingam Arunachalam

has been accepted towards fulfillment  
of the requirements for

Master degree in Materials Science

  
Major professor

Date May 16, 1994

**PLACE IN RETURN BOX to remove this checkout from your record.  
TO AVOID FINES return on or before date due.**

DATE DUE	DATE DUE	DATE DUE
_____	_____	_____
_____	_____	_____
_____	_____	_____
_____	_____	_____
_____	_____	_____
_____	_____	_____
_____	_____	_____

**MSU is An Affirmative Action/Equal Opportunity Institution**

c:\clic\datedue.pm3-p.1

**HYDROGEN CHARGING AND INTERNAL HYDROGEN EFFECTS ON  
INTERFACIAL AND FRACTURE  
PROPERTIES OF METAL MATRIX COMPOSITES**

By

Chidambara Ramalingam Arunachalam

**A THESIS**

Submitted to  
Michigan State University  
in partial fulfillment of the requirements  
for the degree of

**MASTER OF SCIENCE**

Department of Materials Science and Mechanics

1994

James P. Lucas

## **ABSTRACT**

### **HYDROGEN CHARGING AND THE EFFECT OF CATHODIC CHARGED HYDROGEN IN A PARTICULATE - REINFORCED ALUMINUM COMPOSITES**

By

Chidambara Ramalingam Arunachalam

This investigation was conducted to assess the influence of hydrogen on interfacial and bulk fracture properties of Al/SiC composite. Cathodic charging was used to introduce hydrogen into the samples. As a reference hydrogen was introduced into the matrix material Al-6061-T6. To determine the hydrogen concentration in Al/SiC composite a thermal desorption technique was used. In spite of sustained charging periods, the evidence suggested that high hydrogen concentration existed at the surface. Corrosion products and extensive surface cracking were observed on the surface of the composite materials. Fracture surface morphology showed insignificant difference between the charged and the uncharged samples indicating the lack of internal hydrogen penetration into the specimen. Due to hydrogen-induced surface corrosion of charged samples, final ligament fracture was brittle in nature as opposed to uncharged samples which exhibited ductile behavior. In this study emphasis is given to the role of surface hydrogen absorption on failure in Al/SiC composites.

## **ACKNOWLEDGEMENTS**

First and foremost I would like to thank my adviser Professor James P. Lucas for all his encouragement, help and support, without which this work would not have been possible. I would also like to thank my committee members Professor Melissa J. Crimp of the Department of Materials Science and Mechanics and Professor Dennis J. Miller of the Department of Chemical Engineering for their help and suggestion from time to time. Thanks are also due to Professor K. Mukherjee and all other faculty, staff and students of the Department of Materials Science and Mechanics for their support. Last but not the least I would like to thank my guru, parents and brother for their support.

## **TABLE OF CONTENTS**

<b>List of Tables</b>	<b>VI</b>
<b>List of figures</b>	<b>VII</b>
<b>1. Preface</b>	<b>1</b>
<b>2. Introduction</b>	<b>2</b>
<b>3. Background</b>	<b>4</b>
3.1 Hydrogen in Metals (w.r.t Al)	4
3.1.1 Solubility	5
3.1.2 Diffusivity	7
3.1.3 Occupying Sites	11
3.1.4 Trapping	12
3.1.4.1 Vacancies	12
3.1.4.2 Dislocations	14
3.1.4.3 Grain Boundaries	14
3.1.4.4 Precipitates	15
3.1.4.5 Particle- Matrix Interface	16
3.2 Hydrogen Charging	16
3.3 Cathodic Hydrogen in Metals	19
3.3.1 Pure Aluminum	19
3.3.2 Aluminum alloys	20
3.4 Hydrogen Transport by Dislocation	21
3.4.1 Theory	21
3.4.2 Experimental Evidence	23
3.5 Thermal Desorption for Qualitative Measurement of Hydrogen.	25
3.4.1 Theory	25
3.4.2 Basic Operation	25

<b>4.</b>	<b>Experimental Procedure</b>	<b>30</b>
	4.1 Materials	30
	4.2 Cathodic Charging of Hydrogen	30
	4.3 Desorption Experiments	35
	4.4 Characterization of Al-SiC Composite and Decohesion experiment	36
	4.4.1 Mounting the Tensile Samples	36
	4.4.2 Polishing	37
	4.4.3 Microstructural Characterization	37
	4.5 Mechanical Testing	37
<b>5.</b>	<b>Results and Discussion</b>	<b>40</b>
	5.1 Cathodic charging of hydrogen	40
	5.2 Characterization of Al/SiC Composite and Decohesion Experiment	45
	5.3 Fracture Surface Morphology	50
	5.4 Thermal Desorption Experiment	57
	5.5 Mechanical Testing	65
<b>6.</b>	<b>Conclusions and Future Work</b>	<b>78</b>
	<b>BIBLIOGRAPHY</b>	<b>81</b>

## **LIST OF TABLES**

Table 3.1 Solubility data for hydrogen in solid aluminum	6
Table 3.2 Diffusivity data of hydrogen in aluminum	9
Table 3.3 Thermal conductivity of various gases relative to air	26
Table 4.1 Material used in this study	31
Table 4.2 Sample dimensions used corresponding to various tests are tabulated.	38
Table 5.1 Sample dimensions, charging conditions and material used are shown for various desorption curves obtained.	59
Table 5.2 Flexural test results obtained are shown for both the charged and the uncharged samples of Al/SiC.	67
Table 5.3 Tensile test results obtained are shown for both the charged and the uncharged samples. Corresponding sample i.d and material used are also tabulated.	68

## LIST OF FIGURES

Figure 3.1	Cathodic charging apparatus	17
Figure 3.2	Schematic diagram illustrating the working principle of pulse chemisorb 2700	27
Figure 4.1	a). Schematic diagram illustrating the cathodic charging set-up. b). Photographs shows the cathodic charging set-up.	34
Figure 4.2	Design of the three point bend test fixture.	39
Figure 5.0	a). Macrograph shows the crack formed in steel charged with hydrogen. b) Macrograph indicates the absence of crack in the uncharged steel.	41
Figure 5.1	a). Hydrogen-induced corroded surface layer of Al/SiC Composites.	43
Figure 5.1	b) Acquired X-ray spectrum for the corroded surface layer.	44
Figure 5.2	Microstructure of Al/SiC composite a)700X b)2.20KX.	47
Figure 5.3	a) Uniform precipitates of $Mg_2Si$ in the bulk matrix. b) Micrograph shows cracked SiC particles.	48
Figure 5.4	Shows void growth associated with the fractured particles a) 10.0KX b) 1.10KX.	49
Figure 5.5	a). Micrograph showing transparticle fracture, slip bands and microvoid coalescence of the matrix [charged $6\frac{1}{2}$ hours]. b). Fracture surface shows extensive plastic deformation as striations on the inside of the void [charged $6\frac{1}{2}$ hours].	53
Figure 5.6	Shows bottom slip band of figure 5.6 b at higher magnification.	54

Figure 5.7	a). The fracture surface shows a cluster of SiC at higher magnification (no hydrogen). b). Extensive plastic deformation was observed as striations are prevalent on the inside of the void walls as a result of intense slip bands intersection (no hydrogen).	55
Figure 5.8	Fracture surface morphology shows a bunch of SiC particles, microvoid coalescence of the matrix and void growth around the particle for both the charged (for 19 hours) and the uncharged samples [b].	56
Figure 5.9	Desorption signal obtained by heating the empty quartz tube to 723 K.	60
Figure 5.10	Compares the desorption curves obtained for charged and uncharged steel samples.	61
Figure 5.11	Desorption curve obtained for steel charged with hydrogen [Sample i.d: DS1].	62
Figure 5.12	Compares the desorption curves obtained for charged and uncharged Al-6061-T6 samples.	63
Figure 5.13	Compares the desorption curves obtained for charged and uncharged Al/SiC ( $V_f = 10\%$ ) samples.	64
Figure 5.14	Effect of Surface Hydrogen on the Percentage Final Failure Strain for Al-6061-T6 and Al/SiC Composites (Tested in the Transverse Direction).	69
Figure 5.15	Stress-Strain curves obtained for Sample F1 [Al/SiC ( $V_f = 20\%$ )].	70
Figure 5.16	Stress-Strain curves obtained for Sample F2 [Al/SiC ( $V_f = 20\%$ )].	71
Figure 5.17	Stress-Strain curves obtained for Sample B-1 [Al-6061-T6].	72
Figure 5.18	Stress-Strain curves obtained for Sample B-2 [Al-6061-T6].	73
Figure 5.19	Stress-Strain curves obtained for Sample B-3 [Al-6061-T6].	74
Figure 5.20	Compares the Stress-Strain curves obtained for	

	charged and uncharged samples of Al/SiC ( $V_f = 10\%$ ) tested in transverse direction.	75
Figure 5.21	Stress-Strain curve obtained for Sample C5 [Al/SiC ( $V_f = 10\%$ )] tested in transverse direction.	76
Figure 5.22	Compares the Stress-Strain curves obtained for charged and uncharged samples of Al/SiC ( $V_f = 20\%$ ) tested in transverse direction.	77

## **Chapter 1**

### **Preface**

The interaction of materials with their environment is a subject that has been studied for long time. It is imperative to study the behavior of material in any environment before they can be used in that particular environment. Hydrogen is present in many environments, hence it is important to study the interaction of hydrogen with materials.

Interaction between hydrogen and many materials generally result in the degradation of the material's properties. In the case of metals degradation can occur with very small quantities of hydrogen, on the order of atomic parts per million (at.ppm.). As material scientists are developing new materials it is essential to study the behavior of these materials in various environment before they can be widely used. Despite the fact that research has been done for numerous years on this subject, many aspects of internal hydrogen-induced effects are not yet clearly understood and controversy exists still.

## **Chapter 2**

### **Introduction**

Most of the work in the field of hydrogen has focussed on monolithic materials such as iron and titanium alloys and to a lesser extent, aluminum alloys. In contrast, metal matrix composites have received much less attention.

Because of high specific stiffness and high specific strength of metal matrix composites, the application of these materials has increased, significantly displacing their monolithic counterparts. Although much research has been done on mechanical properties of metal matrix composites obtained under benign test conditions, very little mechanical properties data are found for these materials tested under severe environment condition.

One of the objectives of this study is to choose a suitable technique to charge hydrogen and to design a charging cell. The technique used to charge hydrogen in this study was cathodic charging. This study was conducted to assess the influence of hydrogen on interfacial and bulk properties of Al/SiC composite. Both 20% and 10% volume fraction SiC particulates was used. As a reference, hydrogen was introduced into the matrix material Al-6061-T6. Tensile coupons of composite material (both charged and uncharged) were strained to the same extent, polished using a diamond compound on a lapping wheel, and observed for void nucleation at the interface using a Scanning Electron Microscope.

In order to qualitatively measure the amount of hydrogen charged, a thermal desorption technique was used to get the desorption curve for steel, Al-6061-T6 and Al/SiC composite. Desorption curves obtained for

hydrogen charged samples were compared to those of the as-received sample.

Several important conclusions were made from the above study. Although sustained charging times were used, there was significant evidence that absorbed hydrogen resided mostly on the surface. Cathodic charging of hydrogen results in a corrosion product on the surface of the specimen. An extensive fracture morphology study was conducted. In general, fracture surface morphologies showed insignificant differences between the charged and the uncharged samples. This is to be expected considering the lack of internal hydrogen penetration into the specimen. The surface hydrogen effect was manifested only by the unique fracture behavior of the final ligament failure during mechanical testing. The final ligament in the charged samples showed a brittle behavior as opposed to that in the uncharged samples, which exhibited a ductile behavior. For the matrix material (Al-6061-T6), the differences in strain between the charged and the uncharged samples were found to range from 1 to 2%. This due to the combined effect of surface hydrogen and corroded surface layer.

hydrogen charged samples were compared to those of the as-received sample.

Several important conclusions were made from the above study. Although sustained charging times were used, there was significant evidence that absorbed hydrogen resided mostly on the surface. Cathodic charging of hydrogen results in a corrosion product on the surface of the specimen. An extensive fracture morphology study was conducted. In general, fracture surface morphologies showed insignificant differences between the charged and the uncharged samples. This is to be expected considering the lack of internal hydrogen penetration into the specimen. The surface hydrogen effect was manifested only by the unique fracture behavior of the final ligament failure during mechanical testing. The final ligament in the charged samples showed a brittle behavior as opposed to that in the uncharged samples, which exhibited a ductile behavior. For the matrix material (Al-6061-T6), the differences in strain between the charged and the uncharged samples were found to range from 1 to 2%. This due to the combined effect of surface hydrogen and corroded surface layer.

## **Chapter 3**

### **Background**

#### **3.1 Hydrogen in Metals (w.r.t Al)**

For nearly a century, it has been known that hydrogen embrittles metals. Early investigation clearly indicates that hydrogen easily embrittles more open body centered cubic material like iron and steel. From a casting standpoint, unsoundness in casting, mechanical weakness generated by hydrogen and blistering in wrought products has been noted [1]. Dissolution of hydrogen can lead to embrittlement by formation of brittle matrix hydrides. Though much research has been done regarding hydrogen induced porosity they don't give much information about diffusion and solubility of hydrogen [1]. It has also been found that aluminum alloys are susceptible to stress corrosion cracking, which is often attributed to hydrogen embrittlement, even though gaseous hydrogen does not cause any significant embrittlement [2].

The methods that are generally used to introduce hydrogen into the metal are cathodic and gas phase charging techniques. Despite the fact that aluminum has a low hydrogen lattice diffusivity, deep bulk embrittlement has been observed. Diffusivity of hydrogen depends on the trapping propensity at defects in engineered materials. Dislocations have been proposed as one such trap sites to many metals including aluminum. Many studies indicate strong interaction between hydrogen and dislocations but they are not very conclusive [3,4].

### **3.1.1 Solubility**

#### **Pure Aluminum:**

Numerous studies have been conducted into the equilibrium solubility of hydrogen in pure aluminum [5]. Solubility of hydrogen in aluminum is very low. Two methods have been used to measure solubility of hydrogen in aluminum are gas extraction technique and permeation technique.

The gas extraction technique involved successively condensing out the various gas species in progressively colder traps, finally leaving only hydrogen gas. If pressure of this gas is measured along with its known volume, the amount of hydrogen gas originally in the sample can easily be calculated. This technique has been used in numerous studies Eborall and Ransley [6], Ransley and Neufeld [7], Eichenaeur and Pebler [8], Eicheneauer and coworkers [9]. The rate that the hydrogen is outgassed from the sample is indicative of the diffusivity of hydrogen in the sample. The same treatment has often been used to measure specifically the diffusivity of hydrogen in aluminum which is discussed in the later section.

Hashimoto and Kino [5] used permeation technique to measure solubility of hydrogen in aluminum. Though they were specifically interested in hydrogen diffusion in aluminum at high temperatures, they were able to obtain the solubility of hydrogen in aluminum using a mass spectrometer in an ultra high vacuum chamber, the current through the spectrometer was measured. Hydrogen permeation through the specimen was detected by the  $\text{H}_2^+$  ion current and recorded on a recorder. The equilibrium concentration (solubility) was obtained from the stationary ion cur-

rent,  $I$ , given by

$$C = LI/kAD$$

where

$A$  - Exposed area

$L$  - Sample thickness

$k$ - Constant ( $k=N_0/2k$ )

$N_0$ - Number of lattice sites per unit volume

$2k$ - Permeation rate corresponding to the hydrogen ion current of 1A.

Although several works have measured solubility of hydrogen in aluminum, the result do not generally agree [5]. Solubility data for hydrogen in solid aluminum are shown in Table 3.1.

Table 3.1 Solubility data for hydrogen in solid aluminum

$C_0$ (atm <sup>-1/2</sup> )	$E_F$ (kcal/mol)	Reference
$1.48 \times 10^{-4}$	9.5	Ransley and Neufeld
$2.7 \times 10^{-2}$	19.4	Eichenauer and Pebler
$2.2 \times 10^{-3}$	13.9	Eichenauer, Hattenbach and Pebler
$3.1 \times 10^{-3}$	15.1	Eichenauer
$3.4 \times 10^{-3}$	15.5	Edwards and Eichenauer
$2.3 \times 10^{-0}$	23.1	Hashimoto and Kino

$$C = C_0 \sqrt{P} \exp (-E_F/kT)$$

### **3.1.2 Diffusivity**

The diffusion of hydrogen in metals has been measured using various techniques like desorption technique and permeation technique. However, a large scatter in data indicates how difficult it is to determine the diffusivity of hydrogen in metals. A scatter in the measurements may be attributed to the trapping of hydrogen at lattice imperfections such as impurities, dislocations, grain boundaries, etc., and to the influence of different surface conditions. A large degree of discrepancy in H-diffusivity data obtained for metals is due to the difference in surface conditions. The various surface conditions that can affect the diffusivity of hydrogen in metals are

1. Sample pretreatment can lead to differing states of oxide layer. In case of aluminum the oxide layer acts as a barrier to diffusion of hydrogen. Thus the diffusion of hydrogen into the sample can be increased by minimizing the thickness of the oxide layer.

2. The difference in final surface preparation. The diffusivity of hydrogen into the sample depends upon the method of final surface preparation. The various methods that can be used are [10]

- a) Vacuum annealing after heavy cold deformation
- b) Mechanical abrasion using emery or diamond paste
- c) Electrochemical polishing

Mechanical polishing results in large concentration of voids and dislocations which leads to enhanced solubility [10]. Structure resulting from heavy cold deformation cannot be completely annihilated by vacuum annealing. This results in difference in concentration of semi-microscopic

voids and micro-cracks which leads to difference in H-diffusivity [10].

In desorption technique, the procedure generally used consists of assuming a diffusivity and calculating an out-gassing profile. This method is generally limited to high temperature range where desorption rate can be measured. In permeation technique [5] the diffusion of hydrogen in aluminum was measured using a quadrupole mass spectrometer and an ultra-high vacuum system. In their study [5] hydrogen was introduced into specimen by two methods such as gas phase charging and electrochemical charging. Hydrogen permeation through the specimen was detected by the hydrogen ion current and recorded on a recorder. The diffusion of hydrogen in aluminum has been measured at high temperature and room temperature by permeation method. Diffusion data of hydrogen in aluminum are shown in Table 3.2.

It should be noted here that with exception of few most of experiments were conducted using desorption technique and at high temperature. K.Papp [11] have shown that activation energy and pre-exponential factor of the hydrogen diffusion in high purity aluminum are smaller than those of the less pure. The effect of impurities results in a decreases of the diffusivity  $D$ , at the range of temperature investigated.

As mentioned earlier there have been few measurements made in lower temperature range. A major problem in measuring the flux of hydrogen through aluminum is that of low diffusion of hydrogen in aluminum. To overcome this problem a new technique making use of a composite specimen incorporating a very thin layer of aluminum deposited on

Table 3.2 Diffusivity data of hydrogen in aluminum

Material	Method	$D_0$ m <sup>2</sup> /Sec	Q KJ/mol	Literature
99.99% Al	Desorption 633-873 K	$1.1 \times 10^{-5}$	41	Elchenauer [9].
Al 99	Desorption 773-873 K	$1.2 \times 10^{-5}$	61	Andrew
	843-903 K	$2.0 \times 10^{-6}$	50	Matsuo
99.8% Al	Desorption 723-863 K	$2.5 \times 10^{-2}$	90	K.Papp and E.Kovacs-Csetenyi [11].
99.999% Al	Desorption 723-863 K	$1.9 \times 10^{-5}$	40	K.Papp and E.Kovacs-Csetenyi [11].
99.995% Al	Desorption 723-923 K	$1.01 \times 10^{-5}$	47.69	Outlaw, Peterson and Schmid
99.999% Al	Permeation 573-673 K	$2.1 \times 10^{-5}$	59.83	Hashimoto and Kino (1983) [5].
99.995% Al	Permeation 285-328 K	$9.2 \times 10^{-5}$	55.23	Ishikawa and McLellan [12].

$$D = D_0 \exp (-Q/RT)$$

a thicker substrate of a fast diffusing, high hydrogen solubility media. The sandwiches consisted of layers of palladium, iron and aluminum and were formed by vapor deposition onto the iron substrate. To avoid inter-metallic formation between aluminum and palladium the experiments were conducted at room temperature. The measured diffusivities were between  $10^{-15}$  and  $10^{-16}$  cm<sup>2</sup> per second.

T. Ishikawa [12] employed an electrochemical technique. They measured diffusivity of hydrogen in aluminum in the temperature range of 285-328 K. The room temperature measurements showed good agreement with several of high temperature data. It suggested that hydrogen diffusion in solid aluminum is controlled by single mechanism from 300 K up to the melting temperature. Since the vacancy concentration at 300 K was negligible, good agreement between room temperature and high temperature data indicated that vacancy could not play an important role in the diffusion process. Since there was no deviation from Arrhenius linearity observed in this experiment, it implies that trapping was not significant. It should be noted here that this behavior could have occurred because there were not enough trapping sites in the sample used.

Like solubility, diffusivity of hydrogen depend on the trapping propensity at defects in engineering materials. These traps include dislocation cores, grain boundaries, lattice substitutional sites and particle-matrix interfaces. The strength of traps is represented by the binding energy. The most potent trap site are those at particle-matrix interface (e.g: particle matrix Fe<sub>3</sub>C interface with trap energy about 84 KJ/mol). Extending this one would expect that binding energy of Al/SiC interface

in metal matrix composites to be high. Though trap sites will decrease the diffusion of hydrogen in the material at low and ambient temperature the local hydrogen concentration can be increased in the sample significantly higher than in the pure lattice.

### **3.1.3 Occupying Sites**

The two interstitial sites that hydrogen can occupy are octahedral and tetrahedral sites. There is controversy concerning on which site does hydrogen reside, exactly.

Eichenaur [9] measured solubility of deuterium in 99.99% aluminum between 673 and 903 K. He also calculated the solubility of deuterium in aluminum assuming octahedral site occupancy. Both these calculations agreed well leading him to conclude that hydrogen and deuterium occupied octahedral sites in aluminum.

Positive muons are regarded as light isotope of hydrogen and used to investigate several properties of hydrogen in metals. Manninen and Beck [13] used muons to investigate properties of hydrogen in metal. They point out that numerically, the tetrahedral site has been found to be the most stable position for the proton, in agreement with muon results in doped samples [14] and with theoretical calculations [15]. In view of the fact that some theoretical calculations using various potential modeling give very similar energies for the tetrahedral and octahedral sites (within 0.1 e.v). The result concerning the 'priority' of the tetrahedral site may not be conclusive. They conclude that though the energy minimum is at the tetrahedral site, the barrier is extremely low so that energetics seem to

allow an almost free motion of the proton along the cubic diagonal.

Larson and Norskov [15] used a jellium approximation and calculated energy potential for the proton. They found that energy minimum occurred at the tetrahedral site rather than octahedral site.

### **3.1.4 Trapping**

Hydrogen often preferentially occupies particular lattice sites; trapping sites. Several types of sites have been found to trap hydrogen. These traps include dislocation cores, grain boundaries, vacancies, voids, lattice substitutional sites and particle-matrix interfaces. Trapping would be more efficient at lower temperature and has been proposed to explain deviations from Arrhenius linearity in many metal systems [16].

#### **3.1.4.1 Vacancies**

The possibility of hydrogen trapping at a vacancy in aluminum was first suggested by Popovic and Scott [17]. They used non-linear theory to predict that the binding energy between a vacancy in aluminum and a hydrogen to be 1.23 eV.

In most subsequent investigations, a spherical solid model was used [18,19,20]. The results obtained within spherical solid models indicate a preference for octahedral interstitial site contrary to preference of vacancy as suggested by Popovic.

Hashimoto and Kino [5] measured diffusivities of hydrogen through pure aluminum foils. They obtained the migration energy of hydrogen dif-

fusion at high temperature as 0.61-0.62 eV, which was near to the migration energy of a vacancy. The value for  $D_0$  being 0.21-0.26 cm<sup>2</sup>/sec was somewhat larger than that of a vacancy, 0.02-0.1 cm<sup>2</sup>/sec, which was estimated from the concentration of thermal equilibrium vacancies. They suggested that these facts might mean that the diffusion mechanisms are different between high temperature and room temperature. Dissolved hydrogen probably migrates freely through the interstitial sites at room temperature where the hydrogen concentration is much higher than that of the vacancies. On the other hand, at high temperatures where vacancy concentration is large enough to couple with almost all of the dissolved hydrogen, it may diffuse together with a vacancy due to larger binding energy between hydrogen and the vacancy [5]. Such a diffusion mechanism would give an explanation of the measured  $D_0$  being somewhat larger than that of a vacancy because the existence of hydrogen might enhance the lattice vibration around a vacancy [5].

Larson and Norkov [15] calculated the trapping energy of hydrogen to be 1 eV. Their conclusion was that hydrogen is trapped near the tetrahedral site next to a vacancy with a binding energy of about 1eV.

On the other hand, experiments conducted by Ishikawa and Mc.Lellan [12] suggest that hydrogen diffusion in solid aluminum occurs by single mechanism from 300 K up to the melting temperature. The diffusivity measurements failed to show any deviation from linear Arrhenius relationship over temperature range of 285-328 K and other measurements at high temperature range. From the above observation, they conclude that trapping at lattice vacancies was unlikely.

### 3.1.4.2 Dislocations

If hydrogen should be transported by dislocations then at first hydrogen must be trapped at the dislocations. Later, by motion of these traps, hydrogen transport occurs.

Zurek and others [21] proved that dislocation can act as trap by their internal friction experiments. They were able to identify a very strong peak as a result of hydrogen substitution atom pairing, and, a second, less pronounced peak resulting from hydrogen dislocation interaction for 7075-T6 aluminum with deuterium. They later used SIMS to obtain deuterium concentration profiles. Fatigue and cold rolled samples showed a high concentration of deuterium at the surfaces and significant concentration level of deuterium extending into the material much deeper than the observed oxide layer. This observation suggests trapping of hydrogen at defects induced by these treatments, notably dislocations.

### 3.1.4.3 Grain Boundaries

Edward [22] discusses the phenomenon of reversible hydrogen trapping at grain boundaries in super pure aluminum. They measured the hydrogen solubility in 99.99% aluminum between 673 and 903K. They found that there was decline in hydrogen solubility with that of grain growth. The observed decline in solubility should in this case be related to the reduction in grain boundary area accompanying the grain growth. By measuring change in grain boundary area and change in solubility, the grain boundary solubility was calculated as

$$L_{(g.b)} = 1.6 \times 10^{-6} \exp \left[ \frac{(-50640 \text{ J/mol H})}{(RT)} \right] \quad (\text{mol H Atm}^{-1/2} / \text{m}^2 \text{ g.b})$$

Edward and coworkers calculated the binding energy between hydrogen and the grain boundary to be as 34 kcal/mol.

The work of Hardwick [23] showed that the extent of brittle fracture depend on local hydrogen accumulation at grain boundaries and extent of dislocation transport of hydrogen.

#### **3.1.4.4 Precipitates**

Precipitates both in matrix and grain boundaries can act as traps for hydrogen. Schmans [24] studied the role of primary intermetallic particles situated at grain boundaries on the effect of hydrogen penetration. Schmans observed that grain boundary precipitates in Al-Zn-Mg alloys can getter hydrogen away from the boundary; this is very beneficial because hydrogen trapped at specific precipitates would not reduce the cohesive strength of the entire boundary. He also reported  $\text{MgZn}_2$  precipitates show a distinct propensity for promoting hydrogen bubble nucleation. Bubbles were seen to form on grain boundaries that did not contain precipitates but these bubbles were transient and therefore would not provide beneficial trapping that the grain boundary precipitates provided. Thus they concluded that the hydrogen bubbles show affinity for both grain boundary precipitates in overaged microstructures and for primary intermetallic phases.

Christodoulou and Flower [25] reported similar observation in hydrogen embrittlement of Al-6%-Zn-3%-Mg alloy exposed to water at elevated temperature. Nguyen and coworkers [26] observed that in 7075 alloy there is clear tendency for decreasing susceptibility with increasing size of both matrix and grain boundary precipitates. They concluded that

size of matrix precipitates is the most important factor in determining susceptibility to hydrogen embrittlement, while grain boundary precipitates also play role, but to a lesser extent.

In general one can conclude that intermetallic precipitates, both in matrix and grain boundaries are very potent trapping sites for hydrogen.

#### **3.1.4.5 Particle- Matrix Interface**

Like intermetallic precipitates particle-matrix can also serve as traps. Asaoko [27] calculated the binding energy of particle-matrix  $\text{Fe}_3\text{C}$  interface and found it to be very strong of about 84KJ/mol. The binding energy for dislocation cores and grain boundaries are also relatively strong of about 20-60KJ/mol.

### **3.2 Hydrogen Charging**

Methods for hydrogen charging include

1. Cathodic charging.
2. Cathodic charging during tensile testing [Straining electrode test]
3. Gas phase charging technique.

Cathodic charging is the most often used method to charge hydrogen.

Cathodic charging is more effective than other charging methods because of

1. High fugacity of hydrogen
2. The effect of  $\text{Al}_2\text{O}_3$  layer as a barrier for diffusion of hydrogen is minimized in this method.  $\text{Al}_2\text{O}_3$  being an amphoteric oxide reacts with the electrolyte used for charging and hence decreasing its effectiveness as a barrier for diffusion of hydrogen.

Two types of circuit can be used for cathodic charging of hydrogen: current and voltage control. Figure 3.1 shows a general cathodic charging apparatus. Constant voltage source or constant current source can be

used depending upon the type of circuit selected. In case of a constant current source a voltmeter can be used to measure the voltage between the sample and the anode. Generally an acidic electrolyte with a recombination poison is used for cathodic charging of hydrogen.

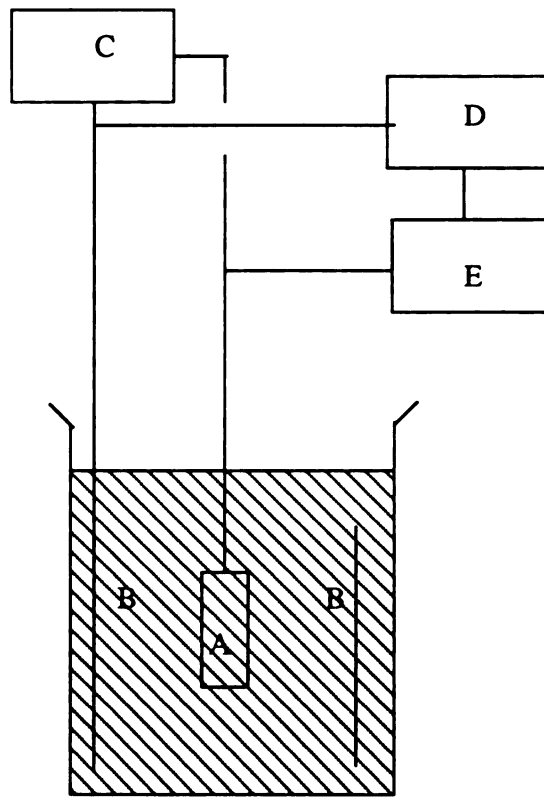


**Figure 3.1 Cathodic charging apparatus.**

**A. Sample, cathode.**

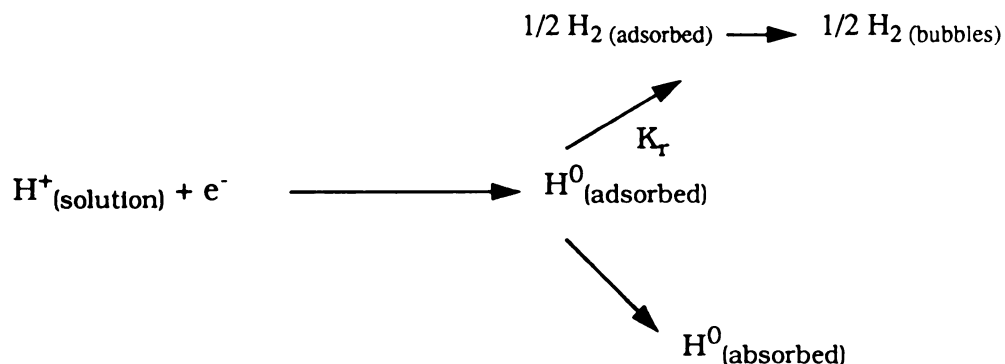
**B. Anode.**

**C. Voltmeter.**

**D. Power source; constant voltage source or constant current source.**

**E. Ammeter.**

First let us examine what a hydrogen recombination poison does. In a typical electrochemical set-up hydrogen ions are attracted to the metal surface where they are neutralized. The resultant hydrogen atoms can either be absorbed by the metal or recombine to form molecular hydrogen, which bubbles off the surface. This process can be represented as



A hydrogen recombination poison slows the rate of formation of  $\text{H}_2$  (adsorbed) from  $\text{H}^0_{\text{(adsorbed)}}$  by reducing the recombination rate constant,  $K_r$ , thus slowing the recombination step leads to absorption of more hydrogen atoms [28]. A number of elements, particularly from groups VA and VIA in the periodic chart, have been identified as hydrogen recombination poisons in metallurgical studies of hydrogen embrittlement. The most commonly used recombination poisons are  $\text{As}_2\text{O}_3$  and  $\text{CS}_2$ . In this study constant voltage source of -1.5V was applied to the cathode (sample). As soon as the voltage is applied, electron is supplied by the anode (platinum wire) and the reduction of  $\text{H}^+$  to  $\text{H}_2$  occurs at the cathode. This molecular hydrogen bubbles off the surface.

Cathodic charging during straining is generally used to investigate the possibility of dislocation transport of hydrogen. The experiment

involves cathodic charging, similar to that described earlier, while the sample is simultaneously strained in tension.

Gas phase charging is done by using Sieverts apparatus. The quantity of hydrogen charged depends on pressure, temperature and time used for charging. The amount of H introduced can be determined by the pressure change in the system [29].

### **3.3 Cathodic Hydrogen in Metals**

Steel and Titanium are the most extensively studied metals for hydrogen embrittlement. Both of these materials are quite sensitive to hydrogen. Beta I and VT-15 titanium alloys are more sensitive to hydrogen when compared to Beta III titanium alloys. For Beta III titanium alloys the percent elongation of tensile specimens is appreciably decreased only by high H contents, much higher than those necessary to embrittle to the same extent other  $\beta$  Ti alloys: Beta I (Ti-13V-11Cr-3Al) and VT-15 (Ti-7Mo-11Cr-3Al), similarly charged and pulled at the same rate [30]. Andler and coworkers concluded that hydrogen redistribution (results in  $H_2$  transport) occurs under the influence of a stress gradient in  $\beta$ -phase titanium alloys. This phenomenon was not observed in  $\alpha$ -phase titanium alloys [31]. The fact that stress induced hydrogen redistribution was not observed in  $\alpha$ -phase titanium alloys is due to the low hydrogen diffusion coefficient in  $\alpha$ -phase titanium at room temperature. Steel being a open structure is easily susceptible to hydrogen embrittlement.

#### **3.3.1 Pure Aluminum**

Watson, Shen and Meshii [32] reported the effects of cathodic charging on pure aluminum. They reported that cathodic charging

decreased the ductility, as measured by strain to failure. All their samples showed a fully ductile fracture modes. They also reported that cathodic charging caused slight hardening in tensile tests.

### **3.3.2 Aluminum alloys**

The most extensively studied aluminum alloy has been 7075. 7050 and 2014 aluminum alloy have also been studied.

Gest and Troiano [2] was the first to study the effect of hydrogen on aluminum alloy. They used high strength aluminum alloy 7071 T651. The embrittlement was found to depend on strain rate and test temperature. The embrittlement was most severe at lower strain rate. They also confirmed the reversibility of hydrogen induced damage. The internal friction experiment obtained a very weak peak at 170K signifying hydrogen-dislocation interaction.

Tehari [33] studied embrittlement of 7075 aluminum alloy in different aging conditions over a range of four orders of magnitude in strain rate. They found that the dependence of embrittlement on strain rate was not constant but rather went through a maximum. The strain rate for maximum embrittlement was different for different aging conditions. They also showed that the recovery at low strain rates was not due to diffusional losses of hydrogen from the sample; they proposed that diffusional escape from detrimental trap sites to more innocuous lattice sites was responsible for the recovery. This explanation was confirmed by the observation that holding the samples in vacuum for 48 hours between charging and testing did not affect the embrittlement [34].

Albrecht, Thompson and Bernstein [35] studied the role of microstructure in hydrogen assisted fracture of 7075 aluminum. For all microstructures (underaged, peakaged and overaged), a temperature dependent loss of ductility due to hydrogen was found. The ductility loss was a function of microstructure, being highest for the underaged and lowest for the overaged material, which suggested a correlation between hydrogen embrittlement and slip planarity. Generally the effect has been explained that overaging increases the number of incoherent precipitates which cannot be sheared by passing dislocations. Underaged microstructure are dominated by coherent shareable precipitates. This explanation has often been used to imply dislocation transport mechanism.

It is important here to mention one aspect of cathodic charging phenomena in aluminum alloys. Albrecht [3] found that most but not all of the embrittlement could be recovered by machining away the surface layer after charging. They suggested that total effect of hydrogen charging must be separated into two smaller effects. One due to a corroded surface layer, and the other associated with embrittling effect of hydrogen retained in interior of the specimen.

Almost all research on aluminum alloy has been confined to 7075 and 2124 alloy. Very few research has been done on 6061 alloy, the material used in this particular study.

### **3.4 Hydrogen Transport by Dislocation**

#### **3.4.1 Theory**

Diffusivity of hydrogen by bulk means is very low. Dislocation transport has been proposed to account for the higher diffusivities seen in

experiments.

The nature of dislocation is that it attracts hydrogen. Although, there is no longer doubt that dislocation sweeping in result deep hydrogen penetration, deeper than by lattice diffusion. The question still remains whether dislocation sweeping can result in significant local enrichment, or supersaturation, of hydrogen at critical failure sites in the material, such as the interface of internal traps. Traps may be precipitate particle interface, grain boundaries and inclusions or internal voids in the material whose interfaces are often preferential site for microvoid or microcrack initiation. It should be noted that microvoid or microcrack can be initiated when a critical hydrogen concentration is exceeded in local regions.

The theoretical basis for quantitatively evaluating any possible supersaturation or enrichment of hydrogen at specific sites in the material as a result of dislocation sweep in of hydrogen was originally laid by two kinetic models.

In one model, by Johnson and Hirth [3], they assume an equilibrium between trapped population and the matrix. If the sink for dislocation-transported atomic hydrogen is a void, then recombination to the molecular state would be expected upon discharge. Hydrogen emission and diffusion away from the void must then be preceded by molecular dissociation. The recombination and dissociation rates are sufficiently high that local equilibrium is established, and is believed to be the most probable situation. Even in the case of annihilation of hydrogen-laden dislocation in a trap free matrix they claim that equilibrium situation will

result. With a equilibrium situation, most of hydrogen leaves the trap and very little supersaturation occurs.

The other model, by Tein [4], contends that internal traps would strip hydrogen off the moving dislocation because of the binding energy of the traps. This would result in supersaturation of hydrogen at the trap-matrix interfaces. Enrichment would occur if the arrival rate of hydrogen to traps by dislocation sweeping were greater than diffusion of hydrogen to surrounding matrix. The model predicted that significant hydrogen build-up can occur at the interface.

Hirth and Dienes [36] on the rate of equilibration of diffusional traps in solids considered the rate at which equilibrium boundary condition is attained at an internal diffusion source. The source is a trap site with a binding energy for the diffusion species relative to the bulk lattice. The case of a given initial amount in the trap and the case where the diffusion species is supplied to the trap at a constant rate are considered. Two types of traps are also considered

1. Short range trap where the binding energy is released in one jump.
2. Long range trap where the binding energy is released in more than one jump.

In their model they concluded that long range trap sites required more time to equilibrate than short range trap sites.

### **3.4.2 Experimental Evidence**

Frankel and Latanison [37] in their experiment observed direct evidence for dislocation transport of hydrogen in nickel single crystal using

the electrochemical permeation modified to allow for simultaneous deformation. The hydrogen flux increased in the easy glide region of deformation even after accounting for the effects of decrease in specimen thickness. At fast strain rate the only explanation for this is dislocation transport. However, it should be noted that polycrystals did not show significant dislocation transport.

Albrecht [38] used straining electrode test to study 7075 aluminum. This test combines straining and cathodic charging. They concluded that combined straining and charging enhances hydrogen embrittlement of an equiaxed HP 7075 alloy, relative to precharging alloy. This observation was consistent across a wide spectrum of aluminum alloys such as 2124 [39] and 7050. In many alloys a microstructure favoring slip planarity has been correlated to high hydrogen susceptibility, generally significant embrittlement is observed in the underaged microstructure. Albrecht [38] found that in HP 7075 for a properly oriented grain structure where significant number of grain boundaries are subjected to normal stresses, the hydrogen induced fracture is primarily intergranular, provided the local concentration is high enough. They concluded from these findings that dislocation transport of hydrogen in aluminum is not only possible, but it is kinetically preferred to volume diffusion. Furthermore, it enhances embrittlement far in excess of that possible by static charging of hydrogen alone.

### **3.5 Thermal Desorption for Qualitative Measurement of Hydrogen.**

#### **3.5.1 Theory**

Chemisorption instrument is generally used by chemist for measuring the density of active sites on the surface of a catalyst. It is also used to measure the total surface area of catalyst or any powdered solid. Here, the instrument is used to measure the amount of hydrogen charged. Though the results obtained are qualitative, they give a very good idea about the amount of hydrogen charged. By calibrating the instrument one will be able to use the instrument to measure the amount of hydrogen charged.

#### **3.5.2 Basic Operation**

Schematic diagram of the instrument is shown in Figure 3.2. A mixture of He/N<sub>2</sub> gas can be used as carrier gas but in this experiment only nitrogen gas was used. This was done to increase the sensitivity for desorption of hydrogen.

The Pulse Chemisorb 2700 has a Thermal conductivity detector (Wheatstone bridge network) which is capable of detecting the difference in thermal conductivity of gas that enters the Quartz tube and the gas that leaves the tube. Nitrogen gas was selected as a carrier gas because nitrogen and hydrogen have good difference in thermal conductivity so that even the presence of hydrogen in small amounts can be detected. Table 3.3 gives thermal conductivity of various gases relative to air. One can see from the table that conductivity of Nitrogen and oxygen are almost the same. This implies that even if there is evolution of oxygen

from the  $\text{Al}_2\text{O}_3$  layer the set-up is not quite sensitive to oxygen.

**Table 3.3 Thermal conductivity of various gases relative to air**

Name	Chemical Formula	Conductivity (Relative to air)
Hydrogen	$\text{H}_2$	7.07
Helium	He	5.84
Nitrogen	$\text{N}_2$	1.00
Oxygen	$\text{O}_2$	1.02
Water vapor	$\text{H}_2\text{O}$	0.67

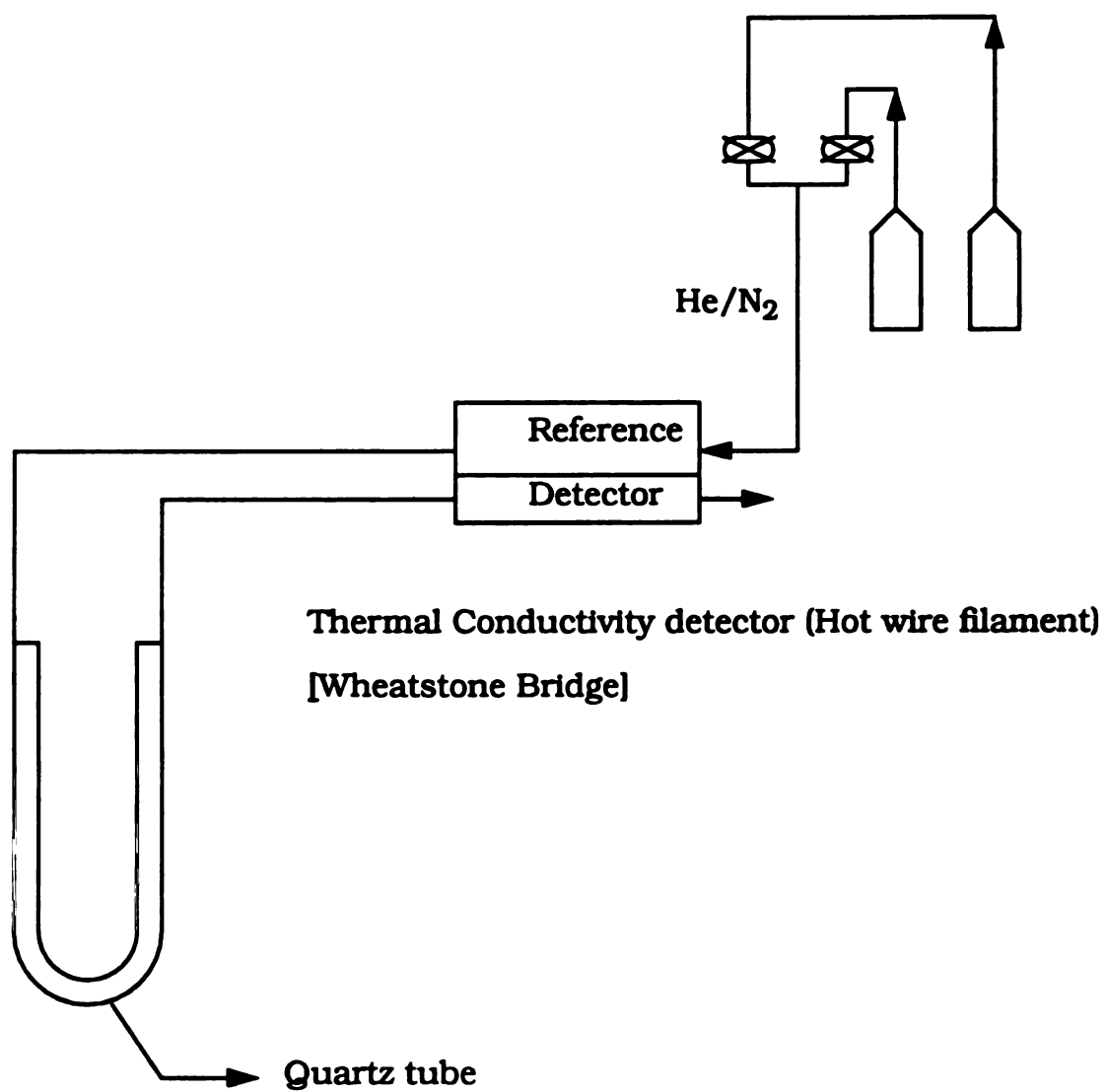


**Figure 3.2 Schematic diagram illustrating the working principle of pulse chemisorb 2700**

A heating mantle was used to heat the quartz tube containing the samples. It is essential here to understand how the Thermal conductivity detector (Wheatstone bridge network) is capable of detecting the difference in thermal conductivity of gas that enters the Quartz tube and the gas that leaves the tube. The Wheatstone bridge network consists of a hot wire filament and the filament is powered by a carefully controlled constant current. When a gas is flown over the hot filament the temperature of the filament changes. It should be noted here that the resistance of the filament changes with temperature. Thus the change in resistance of the filament is controlled by the thermal conductivity of the gas. Hence the resistance of the filament on the way of incoming gas and the resistance of the filament on the way of outgoing gas is going to be different. This difference in resistance of the filaments manifest itself as difference in voltage. In conclusion, the difference in thermal conductivity of gas that enters the Quartz tube and the gas that leaves the tube is given in the output signal as difference in voltage.

There is a display meter which indicates detected output signal. When the analysis gas is more conducting than the carrier gas, depressing the + REL condition push-button below the meter results in a positive display. Using a graphic plotter the detected output signal was recorded with respect to time.

Using the above technique desorption curve (qualitative) was obtained for

1. Steel
2. Al-6061-T6
3. Al/SiC ( $V_f = 10\%$ ).

Steel was first used to test the sensitivity of the instrument for hydrogen desorption. Desorption curves of as received sample and hydrogen charged sample were obtained so that they can be compared. The samples were heated to a temperature of about 718 K. Rate of heating was constant for all the samples. The temperature selected was high enough for hydrogen to desorb. Desorption curves [as received and hydrogen charged] for Al-6061-T6 and Al/SiC ( $V_f = 10\%$ ) were also obtained.

## **Chapter 4**

### **4.0 Experimental Procedure**

#### **4.1 Materials**

Three materials have been used in this study. They are steel, Al-6061-T6 and Al/SiC composite. The SiC particulate composite was supplied by Dural. Two different volume fractions of SiC were considered 10 and 20 pct. The matrix material used is 6061 and is processed by stir casting. The details of the materials are shown in Table 4.1.

#### **4.2 Cathodic Charging of Hydrogen**

To study the effect of internal hydrogen on any properties of materials, hydrogen must be introduced into the material electrochemically [cathodic charging] or thermodynamically [gas-phase charging] depending on the type and condition of the material charged. Our aim is to charge hydrogen in aluminum composites where the presence of passive  $\text{Al}_2\text{O}_3$  layer hinders the diffusion of hydrogen into the material. This problem is more pronounced in gas-phase charging than in cathodic charging. Hence cathodic charging is selected as a method to charge hydrogen into the desired material.

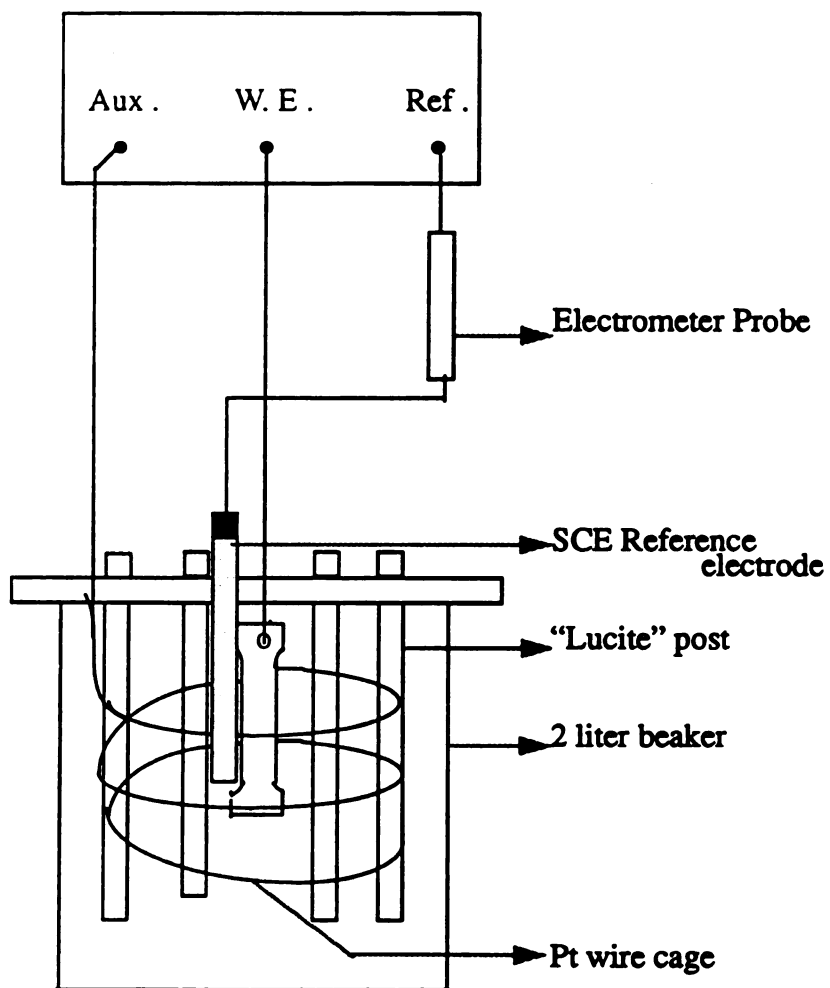
Cathodic charging was accomplished using an acidic electrolyte. For steel acidic electrolyte was made of 5% by volume sulfuric acid solution plus 0.25gm/liter  $\text{As}_2\text{O}_3$  as a recombination poison [28]. For Al-6061-T6 and Al/SiC composite materials acidic electrolyte was made of HCl [pH1] plus 0.25gm/liter  $\text{As}_2\text{O}_3$  as a recombination poison. The specimens were cathodically charged for desired hours under an applied constant potential of -1500mV  $V_s$  standard calomel electrode. The current measured between sample and the anode was between 0.1 to 0.4 A. The current usually started at lower current and increased slowly over the



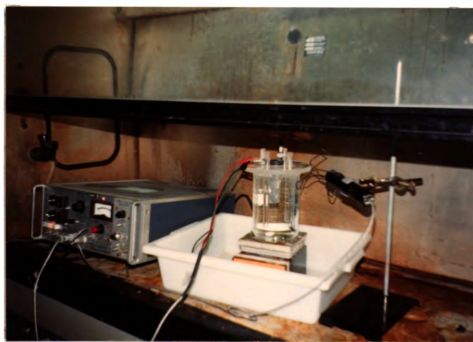
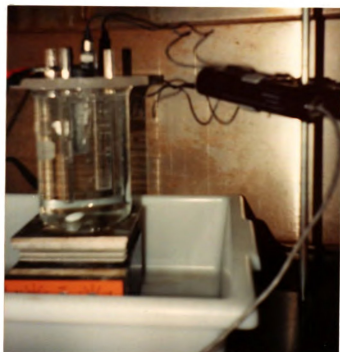
duration of the charging, the increase was likely due to a change in the pH of the solution.

The charging cell contained an anode which consisted of four plastic posts, suspended from a plastic disk. A platinum wire anode was wound outside the post in a single helix. The plastic disk was placed atop a glass beaker which contained the charging solution. The specimen which was the cathode, was suspended from a hole in the center of the plastic disk. The specimen was then in the center of the platinum anode helix. The entire arrangement is shown in Figure 4.1. In the set-up a three electrode cell arrangement is used. The potentiostat is operated in the contr.E mode, the instrument acts as a potentiostat, causing the potential selected by the applied potential/current controls to be maintained between the working and reference electrodes by varying the voltage applied to the counter electrode. The counter (auxillary) electrode can be any chosen electrode desired, because its electrochemical properties do not affect the behavior of the working electrode (sample); it is usually chosen to be an electrode that does not produce substances by electrolysis that will reach the working electrode surface and cause interfering reactions there. Hence in this set-up platinum is chosen as the auxillary (counter) electrode. The electrometer probe monitors the reference electrode potential. It should be understood here that working electrode (sample) is maintained at either virtual or hard ground (zero volts) by the instrument. That is to say, although reference is frequently made to a potential applied to the working electrode, in actual fact the working electrode (sample) is maintained at zero volts, and an opposing potential is applied to the counter electrode (platinum) and detected by the reference electrode.

## Potentiostat



(a)



(b)

Figure 4.1 a). Schematic diagram illustrating the cathodic charging set-up . b) Photographs shows the cathodic charging set-up.

Frequently some parts of sample were painted with etch-resistant lacquer. Since etch resistant lacquer is a non-conducting lacquer the  $H^+$  ions will not go to that surface for reduction. An example of this would be the tensile sample where the non-gauge section were painted with lacquer. This would increase the availability of  $H^+$  ions on the gauge section. Hence the sample is charged with hydrogen more effectively. After charging, before desorption, the samples were rinsed in acetone. Prior to charging the specimens were polished with 600 grit paper so as to decrease the thickness of passive  $Al_2O_3$  layer and specimens were also cleaned with acetone.

After charging, the samples were removed, rinsed in acetone and then immediately they were loaded in MTS system for tensile testing (or any other test performed) or taken in the quartz tube to perform the desorption tests.

#### **4.3 Desorption experiments**

As mentioned earlier chemisorption instrument was used to get desorption curves for both charged and uncharged samples. Small bars of samples of

Length	: 1.85"
Width	: 0.046"
Thickness	: 0.037"

were used. For both charged and uncharged samples, the samples were polished with 600 grit paper so as to minimize the thickness of  $Al_2O_3$  layer. The samples were also cleaned with methanol.

The following procedure was followed to obtain the desorption

curves. Flow controller was switched 'on' and the N<sub>2</sub> cylinder was opened. Regulator pressure was set to off. Now 2700 was switched on. The system was purged with N<sub>2</sub> to remove any air that might be in the system. The detector output was allowed to stabilize for few hours. Now the sample was loaded in the quartz tube. Nitrogen flow rate was adjusted to 5 (10 cm<sup>3</sup>/min). The set-up was allowed to stabilize for 15 to 20 minutes. Peak area was selected to X10 so as to have high sensitivity. Temperature was adjusted to 723K. Chart recorder was turned on to record the desorption curve obtained. Temperature, detector signal output and corresponding time were also recorded.

#### **4.4 Characterization of Al-SiC Composite and Decohesion Experiment**

To study the composite material as such and to study the interfacial decohesion both charged and uncharged samples were strained to the same extent, polished using diamond compound on a lapping wheel and studied using a scanning electron microscope.

##### **4.4.1 Mounting the Tensile Samples**

After straining to the same extent both charged and uncharged samples were mounted on epoxy resin. The samples were mounted on epoxy resin to facilitate polishing. The sample to be mounted was placed on an aluminum foil and was sprayed with mold release. This facilitate the removal of the sample from the epoxy mount after polishing. A ring made of Lucite was placed surrounding the tensile sample, this served as a mould wall. Epoxy resin and hardener were mixed thoroughly in the ratio of 1:1 and poured in the ring before it got cured. Time taken to cure

to solid state was 9 to 12 hours.

#### **4.4.2 Polishing**

The epoxy mounted sample was polished using diamond paste on a lapping wheel for several hours. It should be noted here that the metallography preparation of particle reinforced metal matrix composites is a difficult process. This is because of the extreme difference in hardness of the SiC and Al-matrix material. The samples were first polished with 6 micron diamond paste for two hours, then the samples were polished for several hours using 1 micron diamond paste on nylon cloth. Compound thinner was also used. After polishing the samples were rinsed using methanol and then taken out from the epoxy mount.

#### **4.4.3 Microstructural Characterization**

The polished samples were coated with gold. The gold coated samples (both charged and uncharged) were studied using Scanning electron microscope for decohesion of intermetallic particles, decohesion of reinforced particles and general microstructure characterization.

#### **4.5 Mechanical Testing**

All mechanical tests were performed using Instron or using MTS™ servo-hydraulic test system. A three point bend test fixture was designed so that samples of very small dimensions can be tested (Figure 4.2). To get accurate strain values an extensometer was used during tensile test. Tests were performed at room temperature at a crosshead speed of 0.05 inch/min. After testing the fracture morphology was studied using scan-

ning electron microscope. Table 4.2 gives the detail about sample dimensions used for both tensile and flexural tests.

**Table 4.2** Sample dimensions used corresponding to various tests are tabulated.

Type of testing	Sample I.D	Nominal Sample dimensions	Material used
Flexural test	S1 and S2	Depth = 0.0566" Width = 0.4559" Span = 0.6409"	Steel
Flexural test	F1 and F2	Depth = 0.064" Width = 0.455" Span = 0.640"	Al/SiC ( $V_f = 20\%$ )
Tensile test	B-1,B-2 and B-3	Gauge length= 0.607" Width = 0.5" Thickness = 0.088"	Al-6061-T6
Tensile test	C1,C2,C3 and C4	Gauge length= 0.607" Width = 0.5" Thickness = 0.068"	Al/SiC ( $V_f = 10\%$ )
Tensile test	C5	Gauge length= 0.607" Width = 0.5" Thickness = 0.062"	Al/SiC ( $V_f = 10\%$ )
Tensile test	C6,C7,C8, C9 and C10	Gauge length= 0.75" Width = 0.5" Thickness = 0.065"	Al/SiC ( $V_f = 20\%$ )

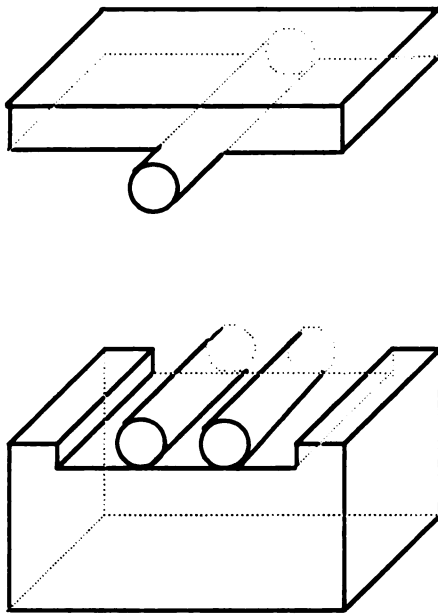


**Figure 4.2 Design of the three point bend test fixture.**

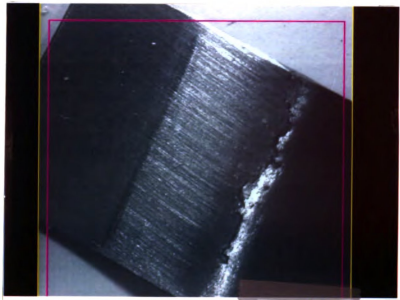
## **Chapter 5**

### **Results and Discussion**

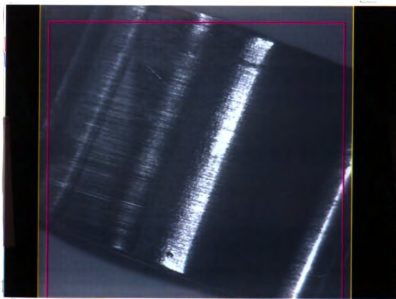
#### **5.1 Cathodic Charging of Hydrogen**

To make sure that the charging setup worked properly, steel samples were charged with hydrogen and flexural test were performed immediately using a three point bend test. The results obtained were compared with the uncharged samples of the same dimension. An indication that charging process is sound is recognized by the presence of hydrogen bubbles around the sample. Two steel samples were simultaneously heated to austenizing temperature range and then quenched in water. This process was done to make the steel more brittle. One of the steel sample was charged with hydrogen and flexural test was performed immediately. The result obtained was compared with the uncharged steel sample. Flexural strain and flexural strength were dramatically reduced for steel charged with hydrogen indicating that the charging setup works properly. Uncharged steel (no heat treatment) was ductile that it did not even crack as opposed to that of the charged steel. Figure 5.0 shows the crack formed in the steel charged with hydrogen.

Steel was selected because steel being a more open structure is more susceptible to hydrogen embrittlement when compared to that of aluminum. Desorption curves and mechanical test results obtained clearly shows that hydrogen can be charged easily into steel when compared to aluminum. The presence of the  $\text{Al}_2\text{O}_3$  layer in case of aluminum acts as a barrier for hydrogen diffusion further reducing the amount of hydrogen charged.



(a)



(b)

Figure 5.0 a). Macrograph shows the crack formed in steel charged with hydrogen (Magnification 10X). b) Macrograph indicates the absence of crack in the uncharged steel (Magnification 10X).

Cathodic charging resulted in a corroded surface layer. Cathodic charged surface of Al/SiC composite was examined using a scanning electron microscope. The micrograph obtained (Figure 5.1) clearly shows the hydrogen-induced corroded surface layer. The spectrum acquired using an energy dispersive analysis of X-ray (EDAX) indicated the presence of aluminum and chlorine in the corroded surface layer (Figure 5.2). Figure 5.1 shows that the corrosive attack follows mainly the grain boundaries, there was also some indication of transgranular cracking. The corroded surface layer was removed by polishing indicating the thickness of corroded surface layer is small. Albrecht and coworkers measured the thickness of corroded surface layer to be around 0.15mm [40]. The result obtained shows that the surface of Al/SiC composite is corroded as a result of cathodic charging similar to that of the results obtained by Albrecht and coworkers [40] in high strength aluminum alloys. Typical of cathodic charging is extensive cracking of corrosion products on the surface of the composite material.

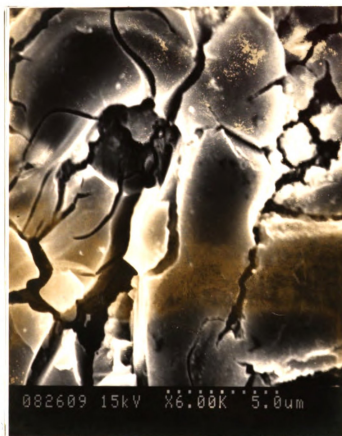


Figure 5.1 a) Hydrogen -induced corroded surface layer of Al/SiC composites.

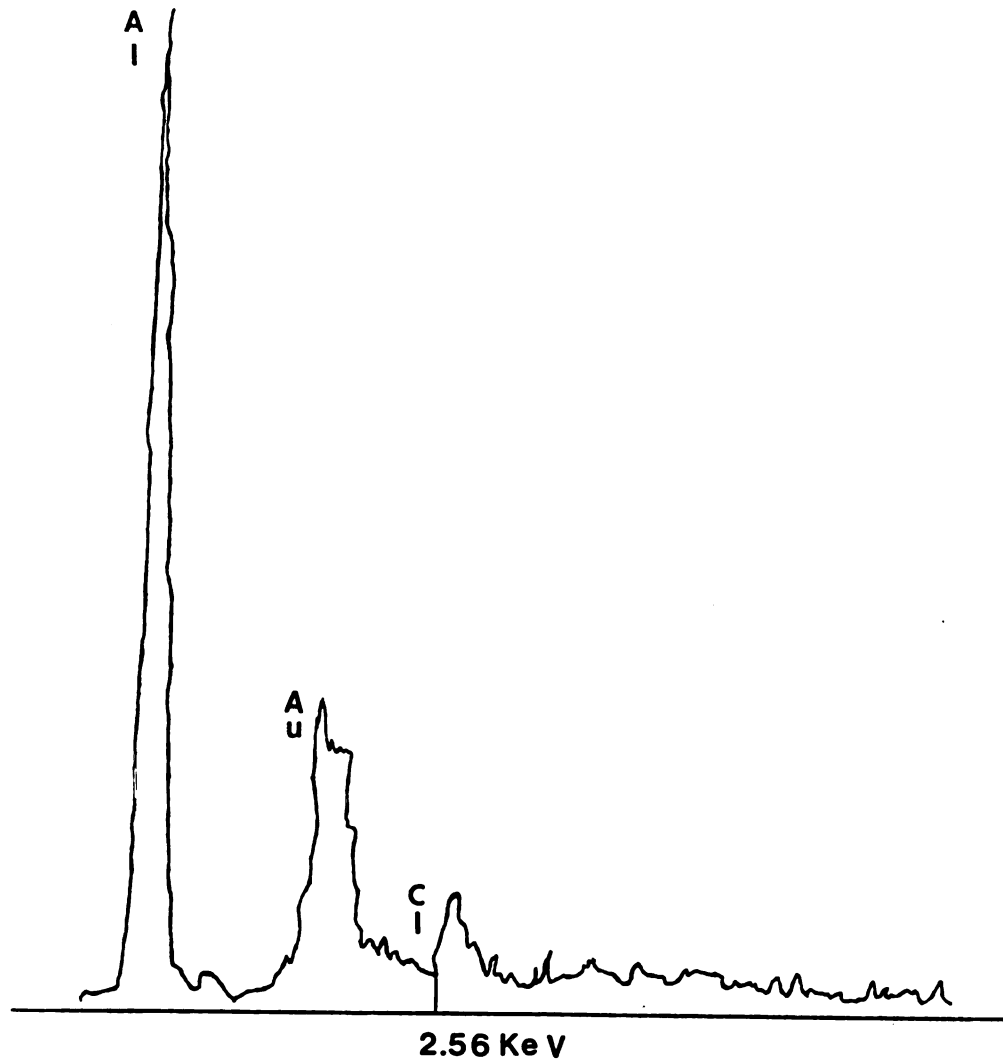


Figure 5.1 b) Acquired X-ray spectrum for the corroded surface layer.

## **5.2 Characterization of Al/SiC Composite and Decohesion Experiment**

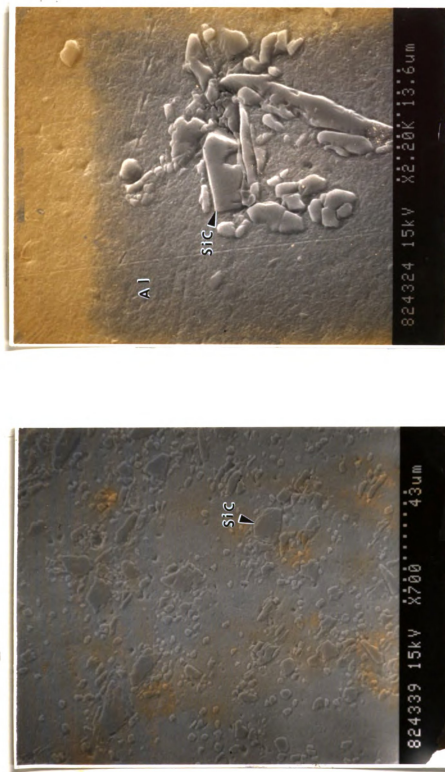
Al/SiC composite consists of matrix metal aluminum and the reinforced particles of SiC. The addition of SiC to aluminum and its alloys confers substantial improvements in specific modulus and strength. However, these improved properties are associated with decrease in ductility and toughness compared with aluminum alloy. The decrease in ductility is evident by comparing the stress-strain curves obtained for Al-6061-T6 with that of stress-strain curves obtained for Al/SiC composites. Figure 5.2 shows the microstructure of Al/SiC composite. The microstructure of Al/SiC composite also exhibited uniform precipitates of  $Mg_2Si$  in the bulk matrix as shown in Figure 5.3 a. It should be noted here that SiC particles are angular whereas  $Mg_2Si$  particles are circular and small.

The failure mechanism observed for the above composite material was similar to the failure mechanism proposed by an investigation conducted by Lucas and others [41]. First the SiC particulates fail by transparticle fracture. Figure 5.3 b shows cracked SiC particles. Fracturing of particulate is the primary fracture process and may be considered as stress controlled process. Figure 5.4 clearly shows such voids formed. Failure of the matrix ligament is a strain controlled process and occurs by microvoid coalescence. The strain controlled process is influenced to a great extent by void nucleation associated with particulates.

Decohesion experiment was performed to study how hydrogen influence the decohesion at particle matrix interface. Tensile coupons of

composite material (both charged and uncharged) were strained to the same extent, polished using diamond compound in a lapping wheel, and observed for void nucleation at the interface using scanning electron microscope. Polished sample did not give rise to a flat surface between the reinforcement and matrix hindering the proper analysis of decohesion at the particle/matrix interface. No clear decohesion was observed at the particle matrix interface for both the charged and the uncharged samples. This indicates there is good bond strength between SiC and aluminum matrix. Flom and Arsenault [42] calculated the interfacial bond strength and inferred from their calculation that debonding of SiC particulates from the matrix (Al-6061-T6) to be a rare event. Interface decohesion will be a rare event if the bond strength is very high when compared to the yield strength of the matrix. No interfacial decohesion was observed by Roebuck [43] in Al-6061/SiC composite material.

Lucas and coworkers [41] clearly show the interface decohesion for A201/SiC metal matrix composite. Thus debonding of SiC from the matrix depends on the type of matrix material used. Polishing was done to remove the corroded surface of the charged sample so that microstructure can be viewed and the influence of hydrogen on the decohesion behavior of the particles from the matrix can be studied. It should be noted here that by polishing one is also removing the mostly heavily charged material. Figure 5.4 shows the ductile fracture occurs by void nucleation at SiC particulates and also at the matrix imperfections ( $\text{Mg}_2\text{Si}$ , inclusions).

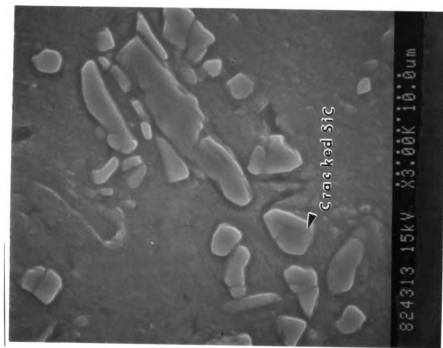


(a)

Figure 5.2 Microstructure of Al/SiC composite a)700X b) 2.20KX.

11

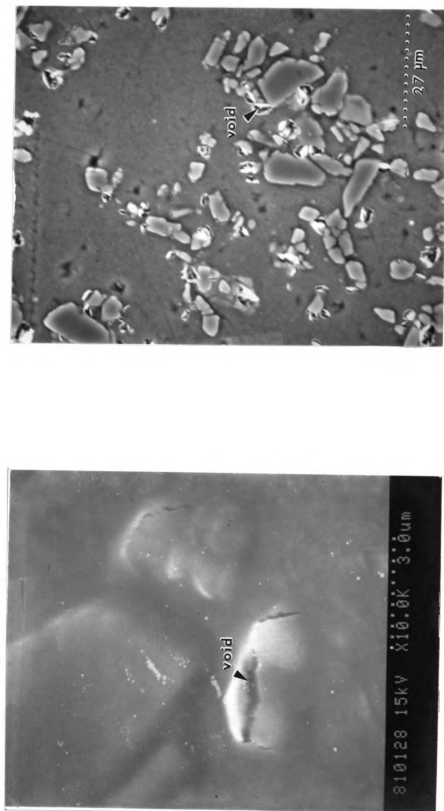
---



(a)

(b)

Figure 5.3 a) Uniform precipitates of  $Mg_2Si$  in the bulk matrix. b) Micrograph shows cracked SiC particles.



(a) (b)  
Figure 5.4 Shows void growth associated with the fractured particles a) 10.0 KX b) 1.10 KX

### 5.3 Fracture Surface Morphology

Fracture surface morphology was studied for

1. 10% SiC charged with hydrogen for  $6\frac{1}{2}$  hours.
2. 10% SiC charged with hydrogen for 12 hours.
3. 20% SiC charged with hydrogen for  $6\frac{1}{2}$  hours.
4. 20% SiC charged with hydrogen for 19 hours.

Fracture surface morphology showed the same mode as reported by Lucas and others [41]. It should be noted here that though Lucas and others studied fracture toughness of the composite using a chevron notch short bar specimen the same fracture phenomenon applies to failure of the composite under tension. The fracture morphology is characterized primarily by deep voids centered around the SiC particles. Ductile failure occur on the matrix ligaments of the fracture process zone by microvoid coalescence in the matrix. Failure in the matrix ligament is a strain controlled process. The ligament between the cracked particles ahead of the main crack failed mostly by shear and microvoid coalescence in the matrix. Fracture of SiC occurred in a multifaceted manner. SiC fracture in a multifaceted manner because of the presence of pre-existing flaws in the particulates.

Figure 5.5 shows transparticle fracture of SiC and shows the presence of large deep void around the SiC particles. The above micrograph also shows microvoid coalescence of the matrix. Fracture mechanism is of the one explained by Ritchie [44]. Failure has been modeled as microvoid coalescence using a stress modified strain criterion originally proposed by McClintock [45] and adopted by Mackenzie and coworkers [46]. The dim-

ple rupture evident is initiated by void nucleation and growth at the SiC reinforcement ahead of the crack tip. The subsequent growth of such voids becomes limited by a plastic shear instability between neighboring voids and the main crack tip, the linkage constitutes crack growth. The instability is caused by localization of strain between large voids and occurs by a fine scale coalescence of microvoids nucleated at constituent phase inclusions in the matrix ligament. Such ductile failure of the matrix can be said as strain induced, in that macrocrack growth by linking of void occurs when critical strain is exceeded ahead of the crack tip. At first, McClintock [45] pointed out that the void growth during ductile fracture is also strong function of the ratio of mean to equivalent flow stress. It also requires the failure criterion for ductile fracture should involve critical strain to be reached over a minimum amount of material rather than at a single point ahead of the crack tip. Accordingly, Mackenzie and others [46] have proposed a criterion for ductile failure where a critical fracture strain ( $\Sigma_f^*$ ) is exceeded over a characteristic distance ( $l_0^*$ ) ahead of the crack tip. It is important to note that critical strain is a function of stress state.

Figure 5.5 also shows the presence of extensive plastic deformation on the inside of the void wall as a result of intense slip band intersection (charged for  $6\frac{1}{2}$  hours). Figure 5.6 shows a closer look at the slip band. Figure 5.7 shows the fracture surface of the uncharged Al/SiC composite. The micrograph shows a cluster of SiC and presence of slip bands on the inside of the void walls. In general, fracture surface morphology showed insignificant differences between the charged and the uncharged sample. This is to be expected considering the lack of internal hydrogen penetra-

tion into the specimen.

The fracture surface micrograph for both the charged and the uncharged sample shows good bond strength between the SiC particles and the aluminum matrix. No fractured interfaces were observed between Al and SiC. Fracture surface showed insignificant difference between the charged and the uncharged samples. It is important here to compare this result with that of the result obtained by You and coworkers [47]. They studied the effect of hydrogen in P/M 2124-20 pct SiC<sub>p</sub> composites and found that void formation and decohesion was observed at the interface. Discrepancy in results is due to

1. You and coworkers [47] used dynamic charging (straining electrode test) of hydrogen. This involves both straining and simultaneous charging. Straining causes dislocation sweeping and dislocation sweeping results in deep hydrogen penetration, deeper than by lattice diffusion.
2. No fractured interfaces was observed even for the uncharged sample in case of Al 6061/SiC composite material whereas some instances fractured interface was observed in Al 2124/SiC composites. This indicates that bond strength between SiC and Al-6061 is good.

Fracture surfaces of charged samples (6 to 12 hours) indicated lack of internal hydrogen penetration into the specimen. To make sure of this observation sustained charging time of 19 hours was used to charge Al/SiC ( $V_f = 20\%$ ). Figure 5.8 compares the charged and uncharged samples of Al/SiC ( $V_f = 20\%$ ). The fracture morphology again indicated insignificant differences confirming the lack of internal hydrogen penetration. Fracture morphology was also analyzed at various position of the fracture surface.

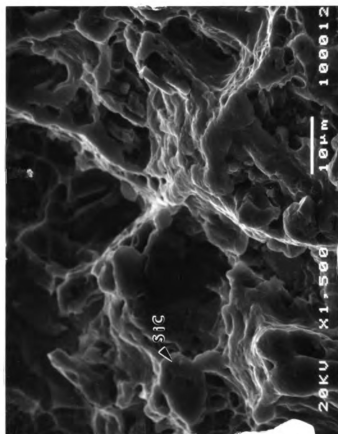
Position



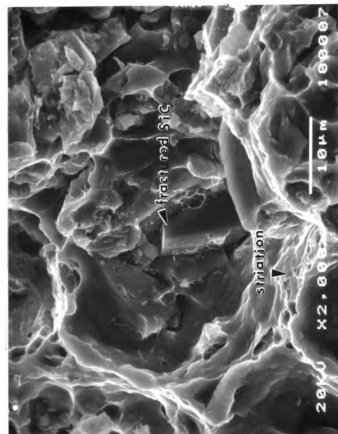
Position



53



(a)



(b)

Figure 5.5 a). Micrograph showing transparticle fracture, slip bands and microvoid coalescence of the matrix [charged  $6\frac{1}{2}$  hours]. b). Fracture surface shows extensive plastic deformation as striations on the inside of the void [charged  $6\frac{1}{2}$  hours].

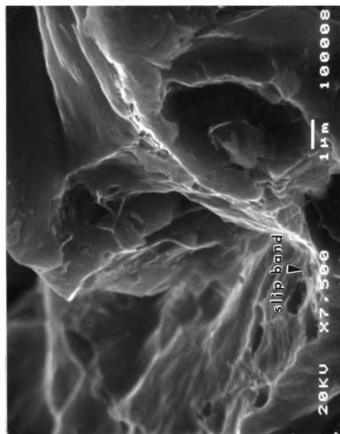
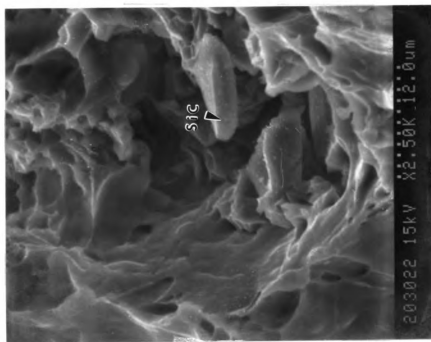


Figure 5.6 Shows bottom slip band of figure 5.5 b at higher magnification.

Position 



Position 

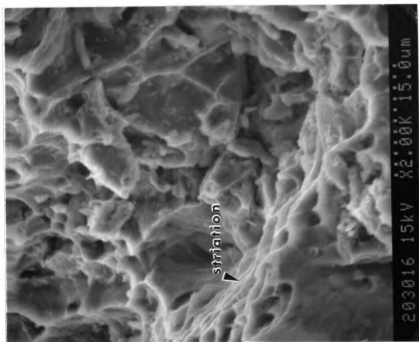
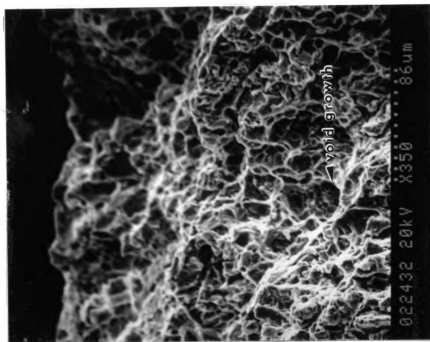
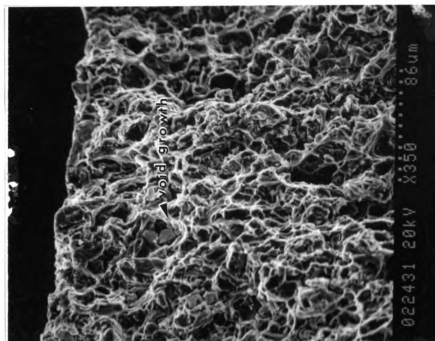


Figure 5.7 a). The fracture surface shows a cluster of SiC at higher magnification (no hydrogen). b). Extensive plastic deformation was observed as striations are prevalent on the inside of the void walls as a result of intense slip bands intersection (no hydrogen).

Position



(a)



(b)

Figure 5.8 Fracture surface morphology shows a bunch of SiC particles, microvoid coalescence of the matrix and void growth around the particle for both the charged (for 19 hours) and the uncharged samples [b].

## 5.4 Thermal Desorption Experiment

Desorption curves were obtained for steel, Al-6061-T6 and Al/SiC composites. Figure 5.10 shows that the amount of desorption signal obtained for steel charged with hydrogen is one hundred times stronger than that of the uncharged steel. This indicates that the Chemisorb 2700 is pretty sensitive for desorption of hydrogen. Figure 5.9 shows the desorption signal obtained by heating the empty quartz tube which can be used as a base reference. Figure 5.12 indicate that the amount of desorption signal obtained for aluminum charged with hydrogen is only slightly higher than the uncharged aluminum. This behavior can be explained by comparing the diffusivity of aluminum (closed packed structure) and steel (open structure).

Ishikawa and Mclellan [48] calculated the diffusivity of hydrogen in 99.99% aluminum at room temperature by permeation method. On the basis of their experiments they calculated diffusivity

$$D = 9.2 \times 10^{-5} \exp - \left( \frac{6651.43}{T} \right) \text{ m}^2/\text{S}.$$

Volkl and Alfeld [43] found the diffusivity of hydrogen in iron to be

$$D = 2.0 \times 10^{-7} \exp - \left( \frac{828}{T} \right) \text{ m}^2/\text{S}.$$

The two important results that are obvious from the desorption curves are

1. Quantity of desorption signal obtained for Al-6061-T6 and Al/SiC is very low when compared to steel.
2. Desorption signal obtained for Al-6061-T6 and Al/SiC (charged

ones) indicate the absence of internal hydrogen in the charged samples.

It is important here to discuss the reason behind the lack of internal hydrogen penetration. As discussed in the background diffusivity of hydrogen in aluminum by bulk means is very low. The various trap sites like dislocation cores, grain boundaries, lattice substitutional sites and particle-matrix interface will further decrease the diffusion of hydrogen into the material. Although the trap sites decrease diffusion of hydrogen in the material the local hydrogen concentration can be increased in the sample significantly higher than pure lattice. The major mechanism by which hydrogen can be transported deeper into the material is by dislocation transport.

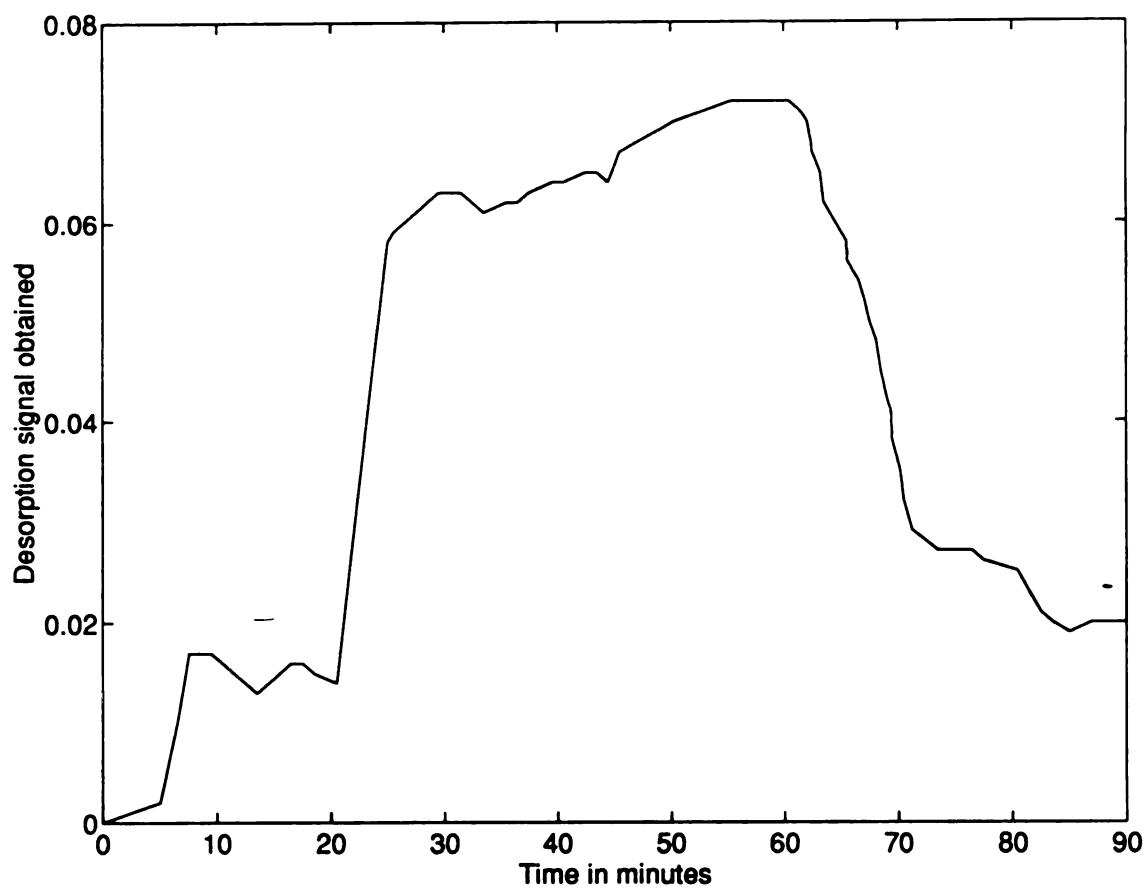
Albrecht [35] used straining electrode test to study 7075 aluminum alloy. They concluded that combined straining and cathodic charging enhance embrittlement far in excess of that possible by cathodic charging alone. From their findings they also concluded that dislocation transport of hydrogen is kinetically preferred to volume diffusion. This observation was consistent across a wide spectrum of aluminum alloys such as 2124 [39] and 7050 alloy. In static charging where there is no straining hydrogen diffuses by bulk means rather than by dislocation transport. The lack of internal hydrogen penetration is attributed to the lack of effective dislocation transport in static charging of hydrogen.

Figure 5.13 compares the desorption curves obtained for the charged and the uncharged samples of Al/SiC ( $V_f = 10\%$ ). Desorption signal of the charged sample is very high initially (for first ten minutes) and

then drops to the level of uncharged samples. The desorption curve of the uncharged is very low initially and then increases after ten minutes and again drops. This indicates that the hydrogen is charged only on the surface of the sample. Table 5.1 gives all information of the material used and the corresponding sample identification.

**Table 5.1** Sample dimensions, charging conditions and material used are shown for various desorption curves obtained.

Sample I.D	Sample Dimensions	Hydrogen/No H <sub>2</sub>	Material used
Figure 5.10	Length = 1.85" Width = 0.046" Thickness = 0.037"	Charged (12 hours) & Uncharged	Steel
DS1 (Figure 5.11)	Length = 1.85" Width = 0.046" Thickness = 0.037"	Charged (12 hours)	Steel
DS2 (Figure 5.12)	Length = 1.85" Width = 0.046" Thickness = 0.037"	Charged (12 hours) & Uncharged	Al-6061-T6
DS3 (Figure 5.13)	Length = 1.85" Width = 0.046" Thickness = 0.037"	Charged (12 hours) & Uncharged	Al/SiC (V <sub>f</sub> = 10%)



**Figure 5.9** Desorption signal obtained by heating the empty quartz tube to 723 K.

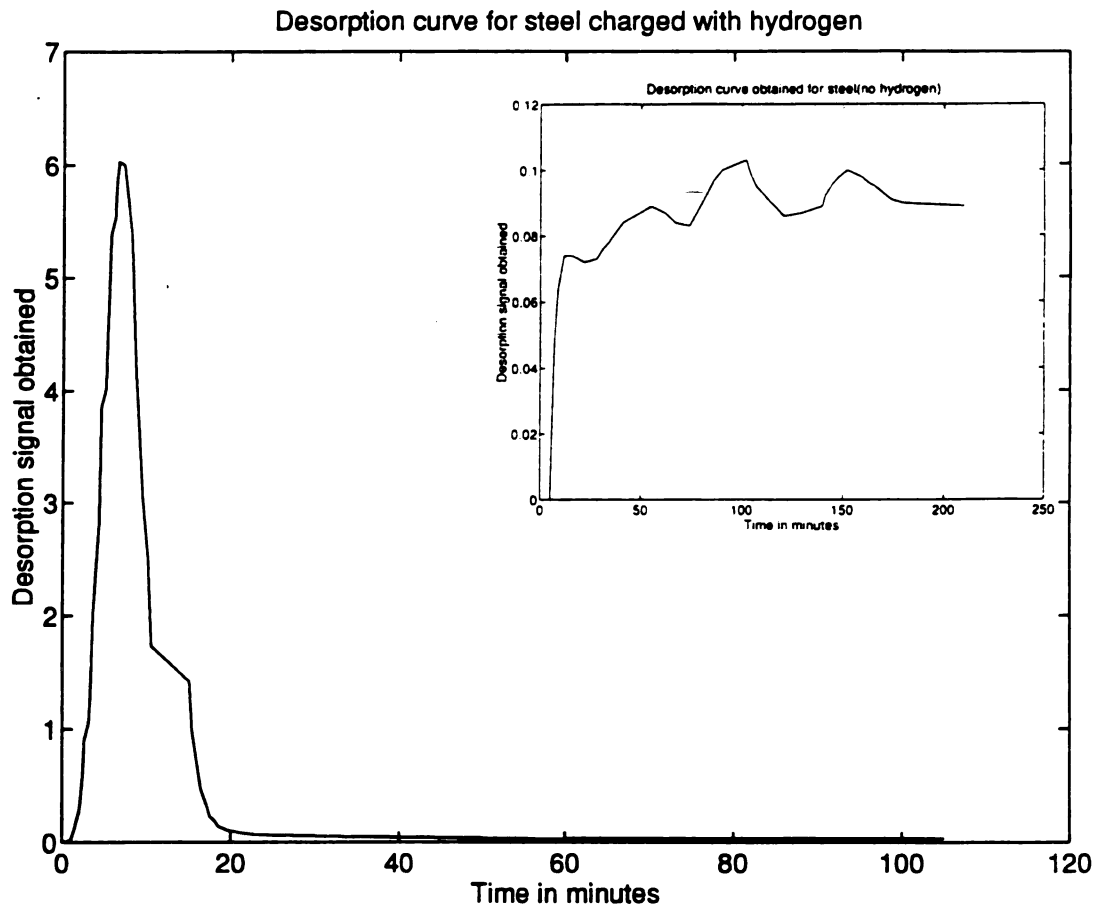


Figure 5.10 Compares the desorption curves obtained for charged and uncharged steel samples.

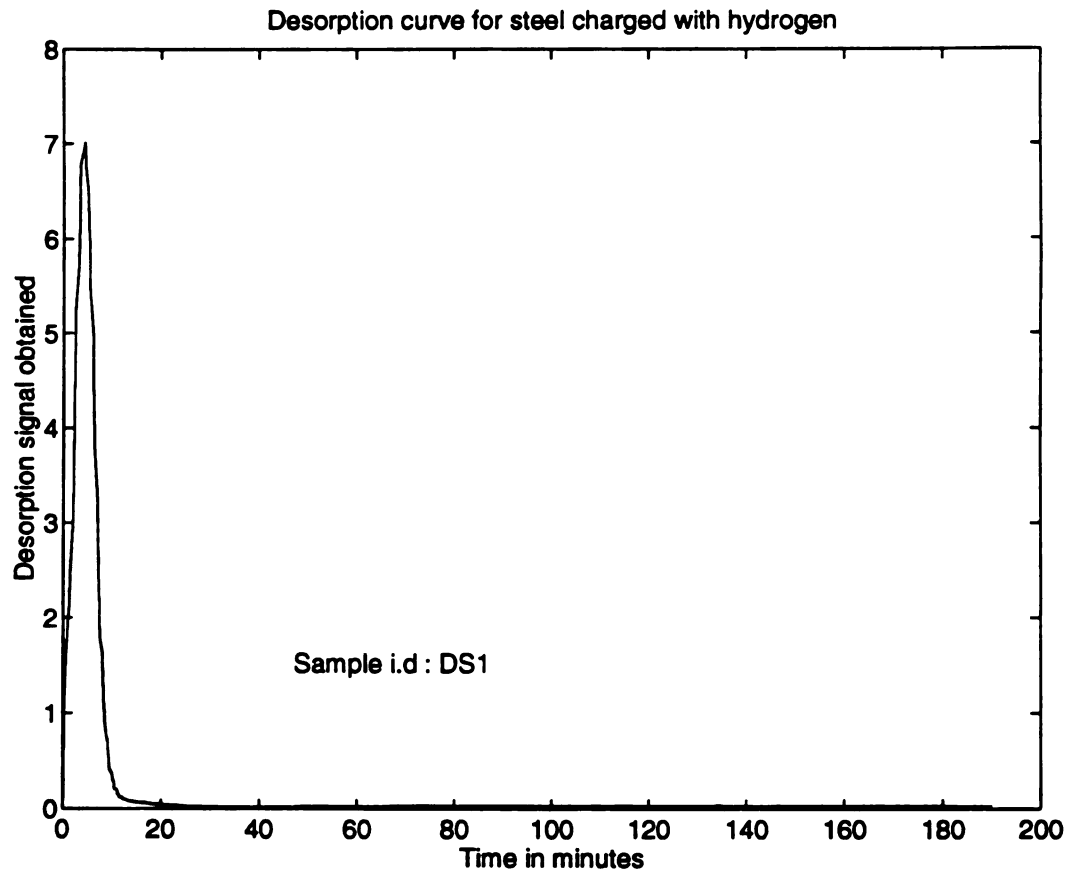


Figure 5.11 Desorption curve obtained for steel charged with hydrogen [Sample i.d: DS1].

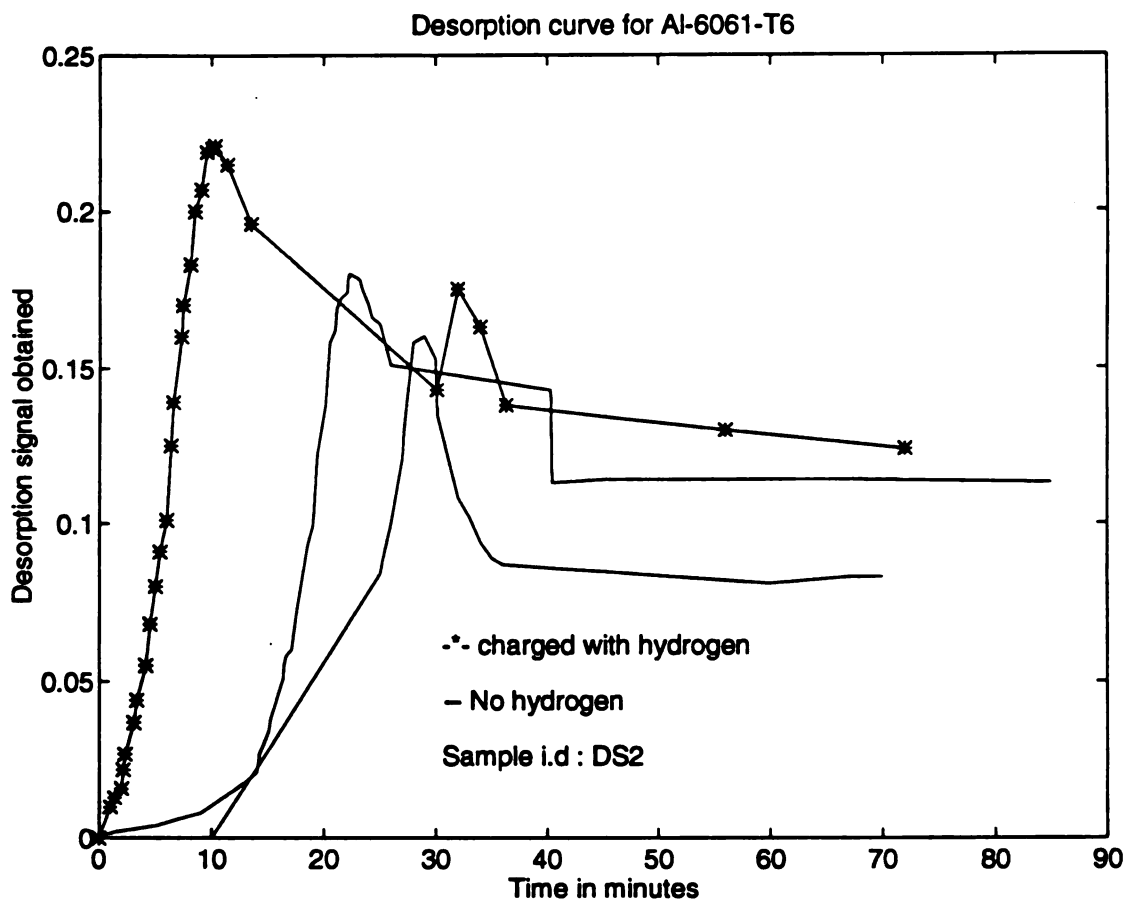


Figure 5.12 Compares the desorption curves obtained for charged and uncharged Al-6061-T6 samples.

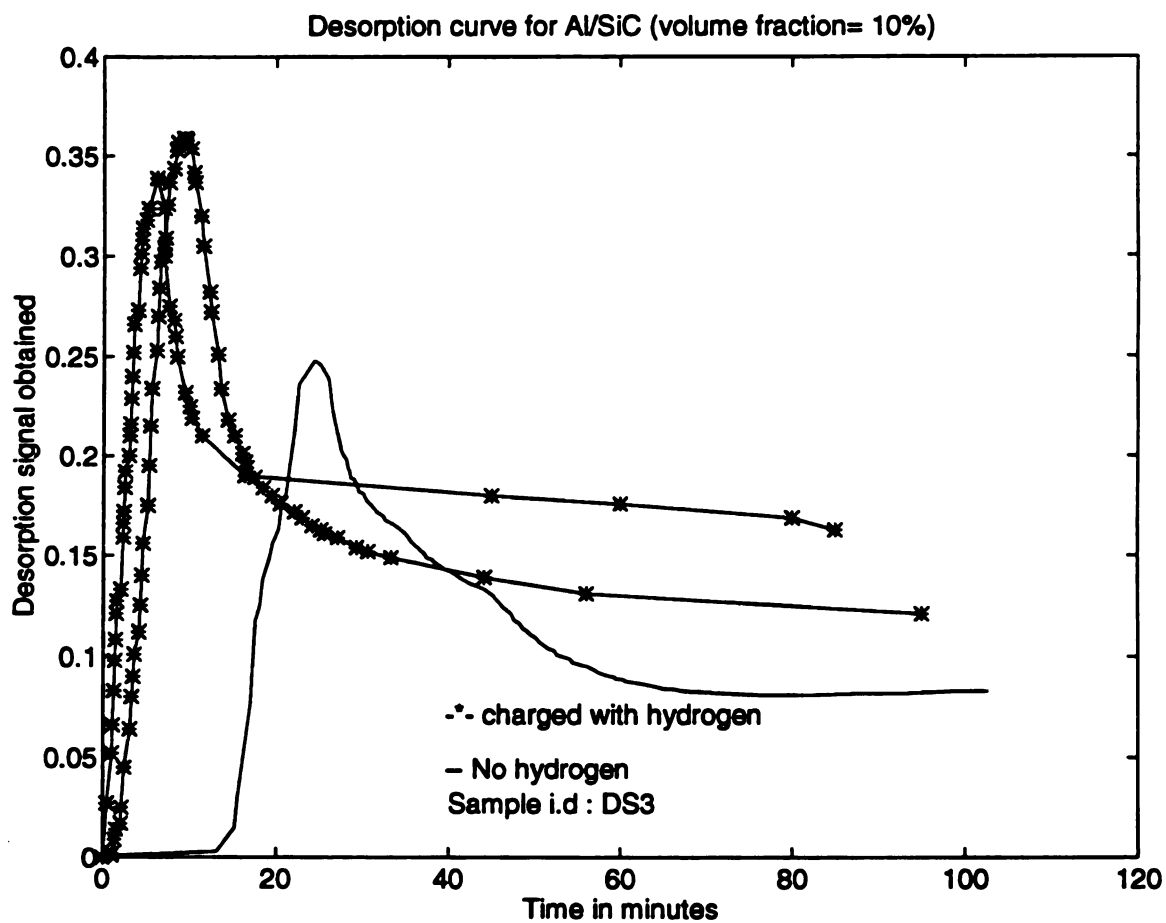


Figure 5.13 Compares the desorption curves obtained for charged and uncharged Al/SiC ( $V_f = 10\%$ ) samples.

### **5.5 Mechanical Testing**

To study the effect of hydrogen in Al/SiC composites, tensile tests and flexural tests were performed. The results obtained are shown in Table 5.2 and Table 5.3. The stress-strain curves obtained are shown in

1. Figure 5.15 to figure 5.16 (flexural tests).
2. Figure 5.17 to figure 5.23 (tensile tests).

It is clearly evident from the stress-strain curves obtained for Al/SiC composites, the hydrogen effect was manifested only in the final ligament fracture of the samples. The ligaments in the charged samples with a corroded surface showed a brittle behavior as opposed to that in the uncharged samples which exhibited ductile behavior. Since only the final ligament fracture behavior was altered it clearly shows the lack of internal hydrogen in the composite samples. Effect of surface hydrogen on the final failure strain% for Al-6061-T6 and Al/SiC composites (tested in transverse direction) is shown in figure 5.14.

Ductility of SiC/Al composites, as measured by strain to failure is reduced with increasing reinforcement content. Figure 5.14 shows the effect of reinforcement content on the behavior of composite material. For uncharged Al/SiC ( $V_f = 20\%$ ) the average final strain is 8.1%, approximately 2% less than that of Al/SiC ( $V_f = 10\%$ ). Composite specimens with low reinforcement contents of 10% volume fraction SiC mostly showed (macroscopically) 45 degree chisel point type of fracture across the width of the specimen. At reinforcement contents (~ 20 volume percent) a 45 degree chisel formed at one edge and extended about half-way through

the width of the specimen but then became flat.

This is similar to observation made by McDanel [49] showing the relation between reinforcement content and fracture modes. By comparing Figure 5.20 and Figure 5.22 one can see that the ultimate strength increased with increasing reinforcement content. Considering the small thickness of samples used it is understandable that there is only small increase in ultimate strength. By carefully examining the two figures one can also see that as the reinforcement content is increased, the stress-strain curves enter the plastic flow region at a higher flow stress. David McDanel [49] indicates that the strength increase was probably caused by closer packing of the reinforcement and smaller interparticle spacing in the matrix. Although the stress-strain curves for Al-6061-T6 were reproducible, for Al/SiC composite a broad range of strain was obtained. This is due to the following reasons

1. Unavoidable differences in the surface preparation.
2. Given the small thickness of the samples the difference can be attributed to the difference in distribution of reinforcement particles (SiC).
3. Unavoidable differences in the quantity of hydrogen charged.

The results obtained indicate that the difference between the charged and uncharged samples (both for Al-6061-T6 and Al/SiC) is due to hydrogen-induced surface corrosion phenomenon.

**Table 5.2 Flexural test results obtained are shown for both the charged and the uncharged samples.**

Sample I.D	Hydrogen/ No hydrogen	Final fracture strain%	Peak Stress (MPa)	Material used
F1	Uncharged	5.0	308	Al/SiC ( $V_f = 20\%$ )
F1	Charged	4.75	238	Al/SiC ( $V_f = 20\%$ )
F2	Uncharged	5.1	340	Al/SiC ( $V_f = 20\%$ )
F2	Charged	4.4	209	Al/SiC ( $V_f = 20\%$ )

Table 5.3 Tensile test results obtained are shown for both the charged and the uncharged samples. Corresponding sample i.d and material used are also tabulated.

Sample I.D	Hydrogen/ No hydrogen	UTS (ksi)	Final fracture strain%	Material used
B-1	Uncharged	49.62	17.06	Al-6061-T6
B-1	Charged	49.87	15.86	Al-6061-T6
B-2	Uncharged	49.62	17.67	Al-6061-T6
B-2	Charged	49.62	16.10	Al-6061-T6
B-3	Uncharged	49.62	17.3	Al-6061-T6
B-3	Charged	49.38	16.3	Al-6061-T6
C1	Charged	17.93	7.28	Al/SiC ( $V_f = 10\%$ )
C2	Uncharged	17.44	9.39	Al/SiC ( $V_f = 10\%$ )
C3	Charged	18.4	10.68	Al/SiC ( $V_f = 10\%$ )
C4	Uncharged	18.4	11.98	Al/SiC ( $V_f = 10\%$ )
C5	Uncharged	16.46	8.53	Al/SiC ( $V_f = 10\%$ )
C6	Charged	18.18	5.94	Al/SiC ( $V_f = 20\%$ )
C7	Uncharged	18.42	7.67	Al/SiC ( $V_f = 20\%$ )
C8	Uncharged	18.91	8.62	Al/SiC ( $V_f = 20\%$ )
C9	Charged	18.18	7.41	Al/SiC ( $V_f = 20\%$ )
C10	Charged	18.42	7.5	Al/SiC ( $V_f = 20\%$ )

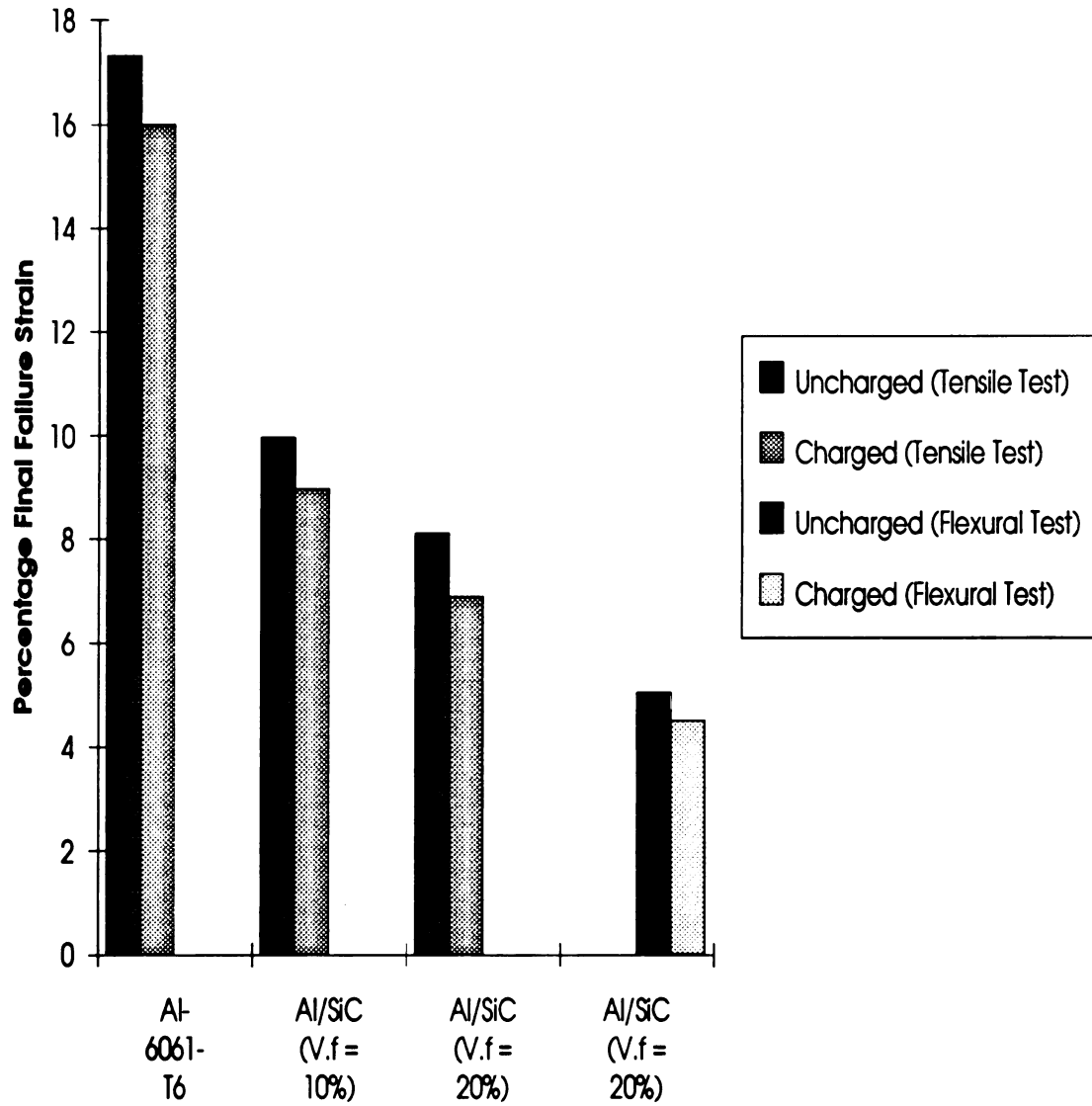


Figure 5.14 Effect of Surface Hydrogen on the Percentage Final Failure Strain for Al – 6061 – T6 and Al/SiC Composites (Tested in the Transverse Direction)

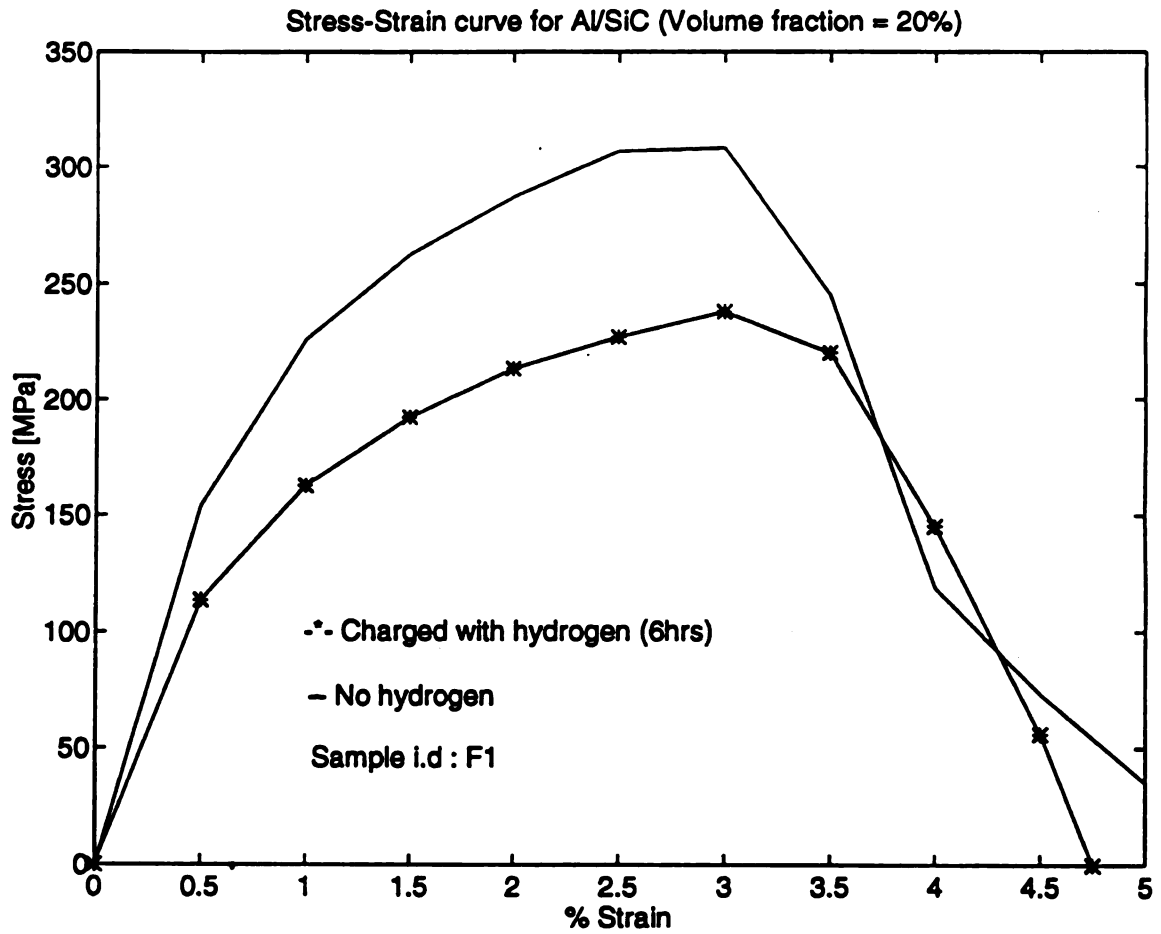


Figure 5.15 Flexural Stress-Strain curves obtained for Sample F1 [Al/SiC ( $V_f = 20\%$ )].

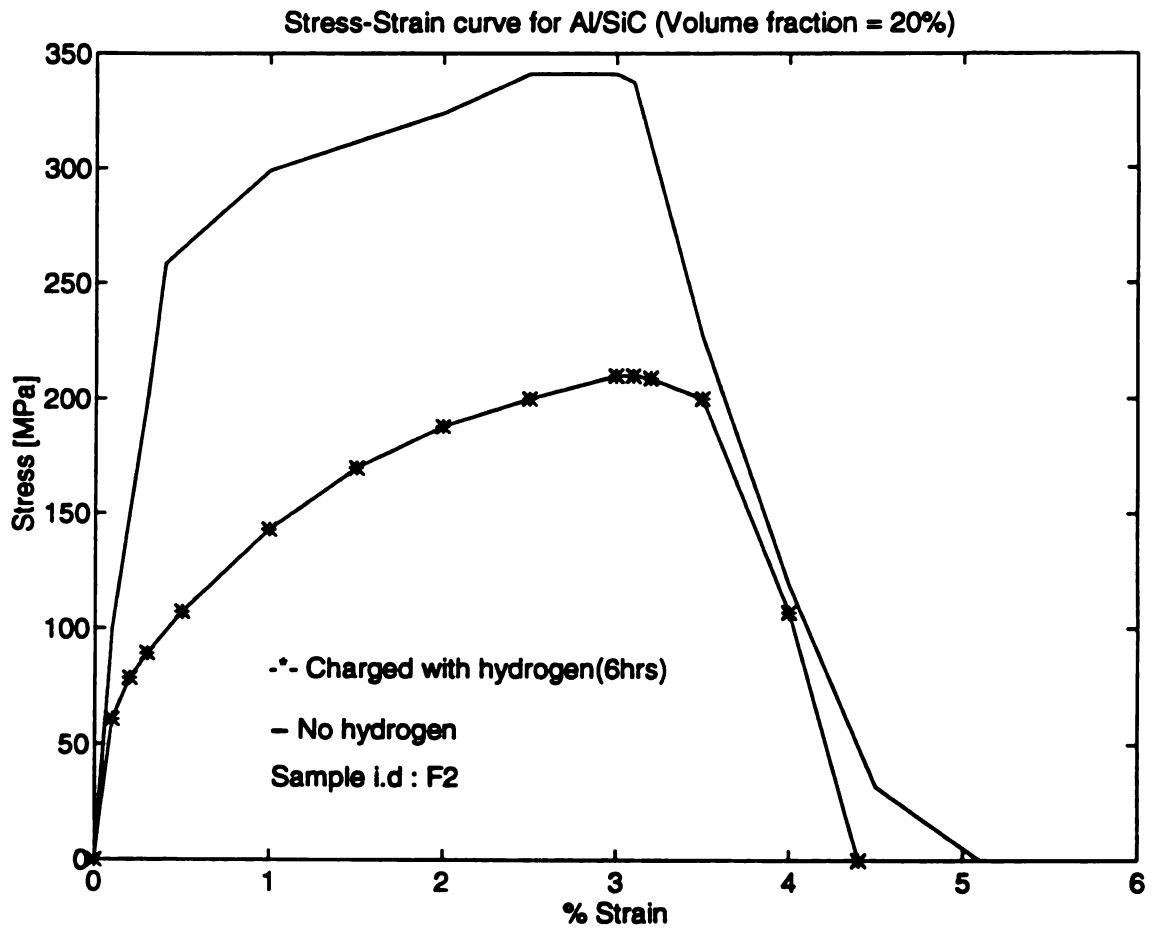


Figure 5.16 Flexural Stress-Strain curves obtained for Sample F2 [Al/SiC ( $V_f = 20\%$ )].

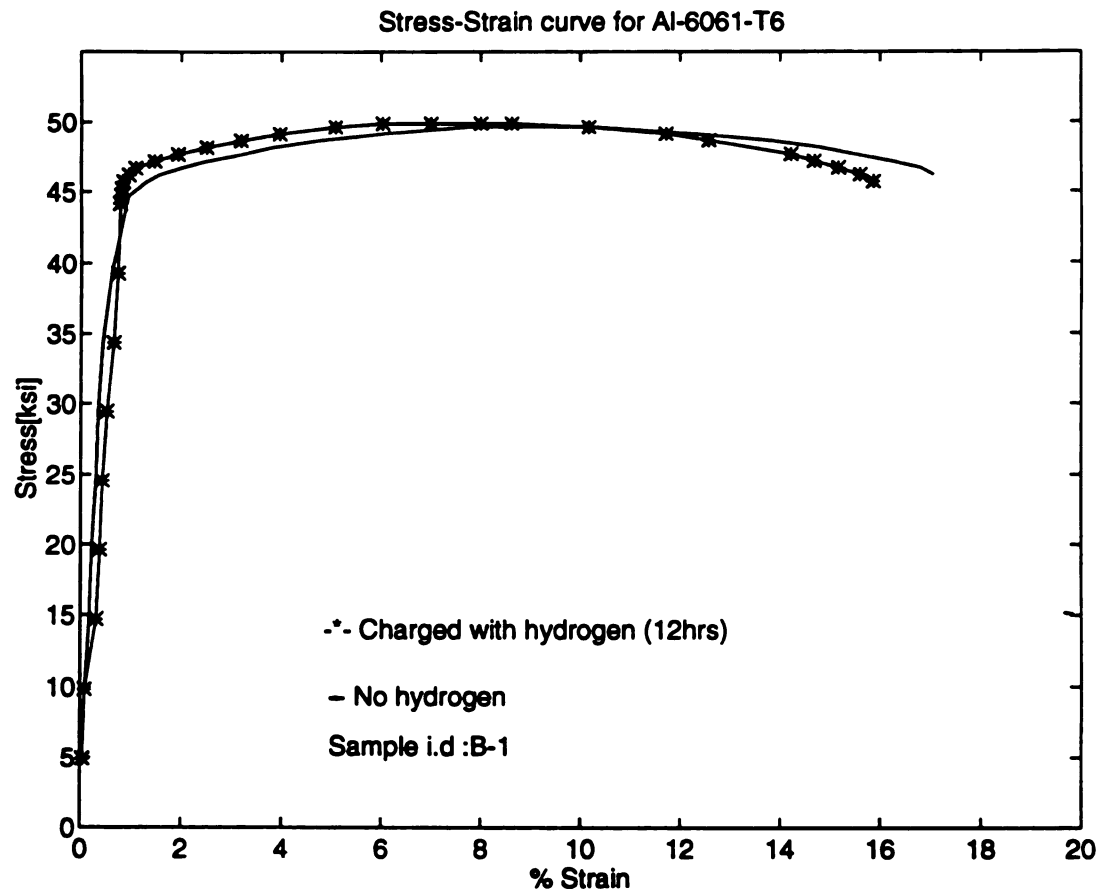


Figure 5.17 Stress-Strain curves obtained for Sample B-1 [Al-6061-T6].

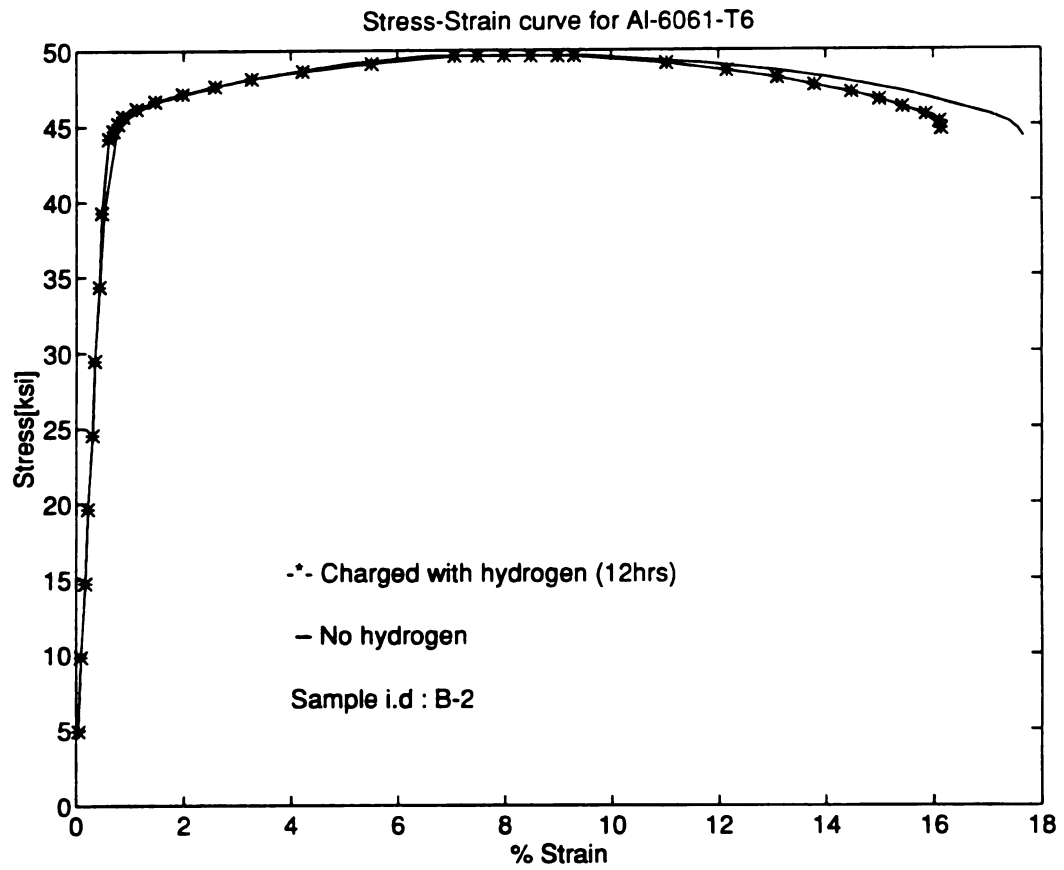
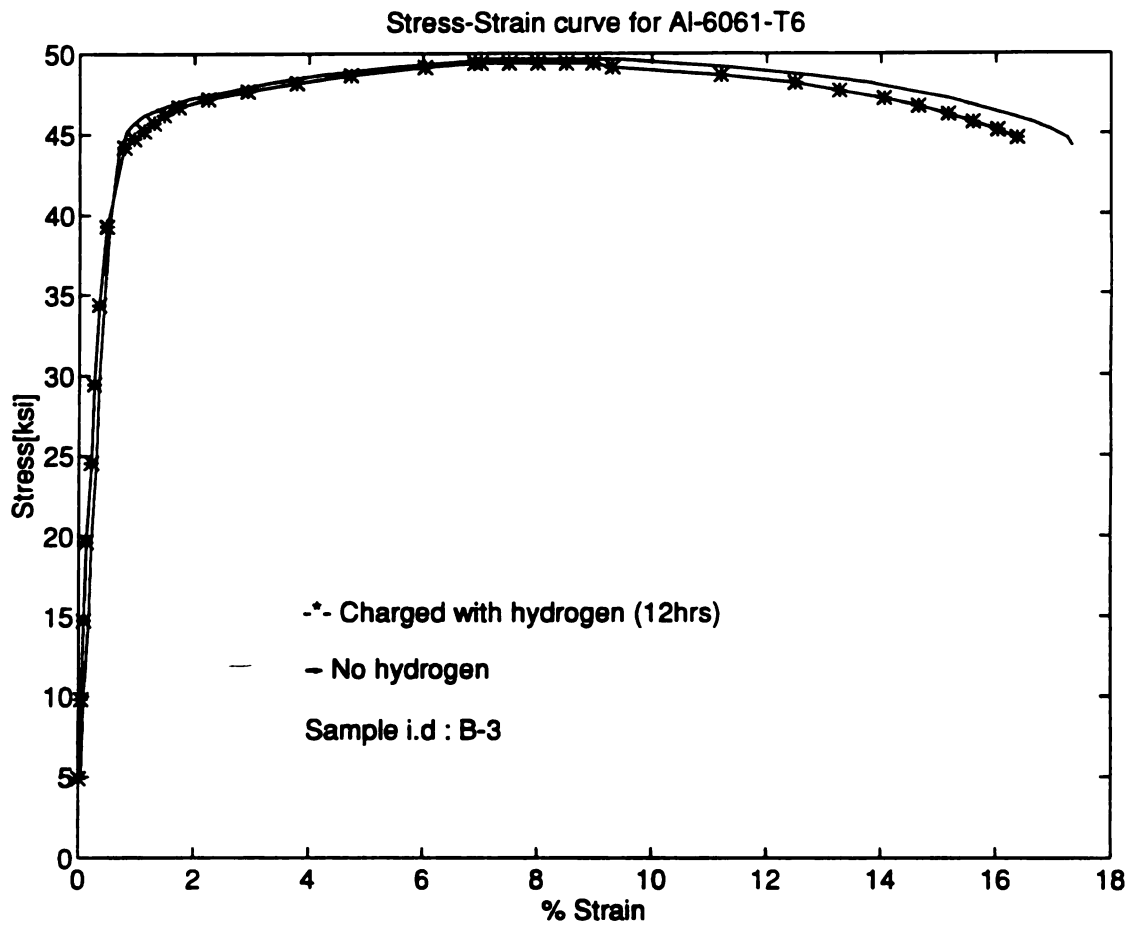


Figure 5.18 Stress-Strain curves obtained for Sample B-2 [Al-6061-T6].



**Figure 5.19 Stress-Strain curves obtained for Sample B-3 [Al-6061-T6].**

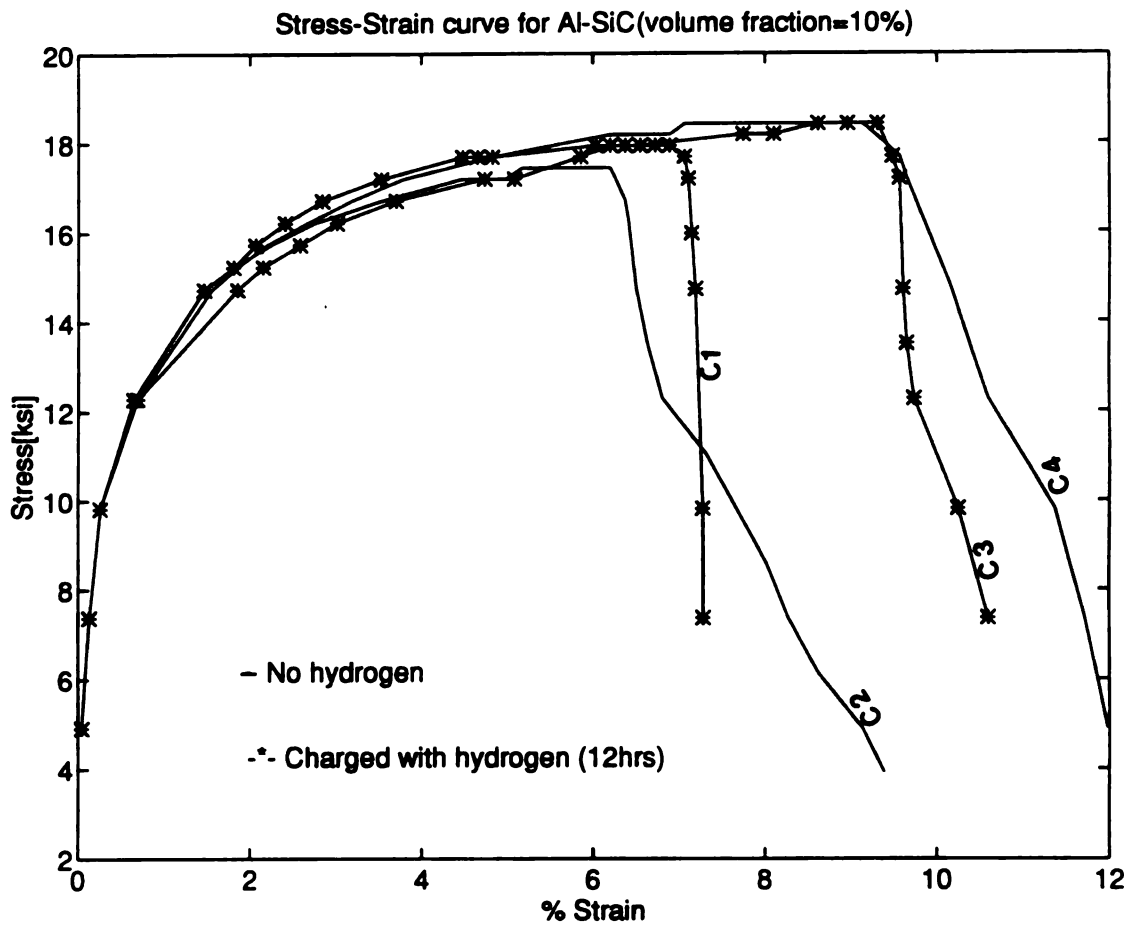


Figure 5.20 Compares the Stress-Strain curves obtained for charged and uncharged samples of Al/SiC ( $V_f = 10\%$ ) tested in transverse direction.

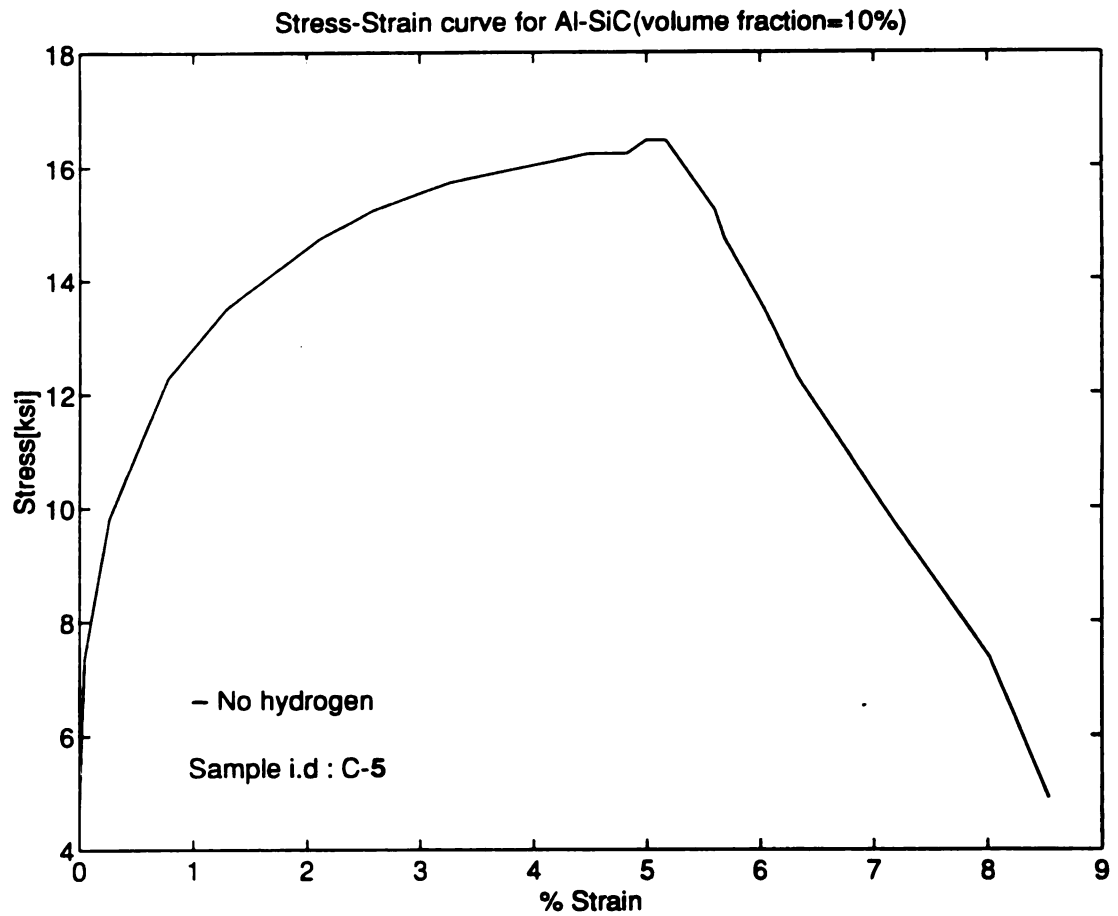


Figure 5.21 Stress-Strain curve obtained for Sample C5 [Al/SiC ( $V_f$  =10%)] tested in transverse direction.

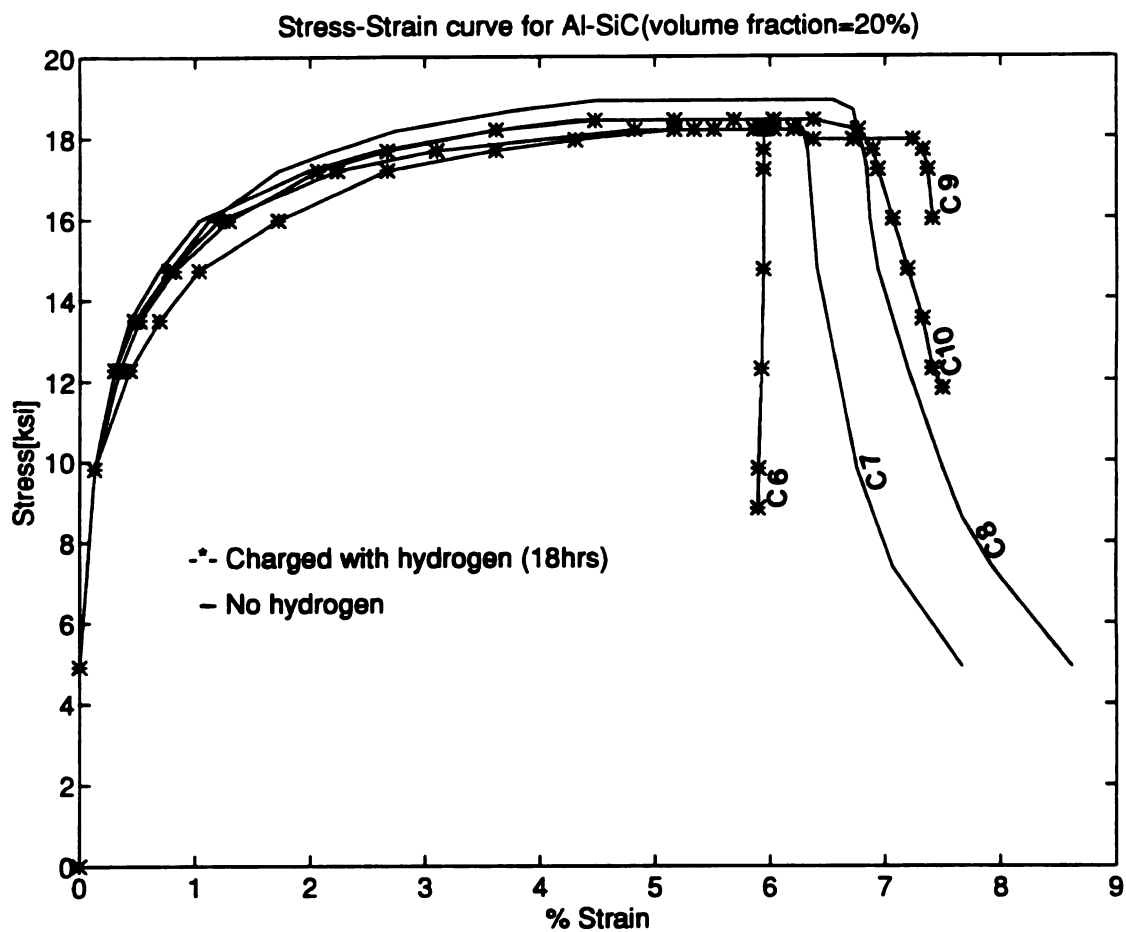


Figure 5.22 Compares the Stress-Strain curves obtained for charged and uncharged samples of Al/SiC ( $V_f = 20\%$ ) tested in transverse direction.

## **Chapter 6**

### **Conclusions and Future work**

**This study has shown several features of the interaction between hydrogen and Al-6061-T6 and Al/SiC composites.**

- 1. A cathodic charging cell was designed so that hydrogen can be charged into any material desired.**
- 2. A thermal desorption technique was used to determine the hydrogen concentration in steel, Al-6061-T6 and Al/SiC composite materials. The desorption curves obtained indicate that high hydrogen concentration existed at the surface even for prolonged charging times (12 hours). This clearly indicates that cathodic hydrogen interaction with Al-6061-T6 and Al/SiC composites is of a surface phenomenon rather than that of the bulk.**
- 3. Cathodic charging of hydrogen results in corrosion of the surface layer of Al/SiC composites.**
- 4. Extensive fracture morphology study was conducted. In general, fracture surface morphology of Al/SiC showed insignificant difference between the charged and the uncharged samples. This signifies the lack of internal hydrogen penetration into the specimen. The fracture surface morphology study also gives a clear picture of the mechanism of fracture of Al/SiC composite materials.**
- 5. The surface hydrogen effect was manifested only by the unique**

fracture behavior of the final ligament failure during mechanical testing. This is clearly evident from the stress-strain curves obtained for Al/SiC composites (both flexural and tensile tests). Due to hydrogen- induced surface corrosion of charged samples, final ligament fracture was brittle in nature as opposed to uncharged samples which exhibited ductile behavior.

6. For Al-6061-T6 the difference in percentage strain to failure between the charged and the uncharged samples ranged from 5 to 8%.

7. General microstructure characterization of Al/SiC composite was conducted using scanning electron microscope. The various micro-graphs obtained shows that fracture process of Al/SiC occurred by

- a) Failure of the reinforcement by transparticle fracture.
- b) Ductile failure in the interparticle ligament by void coalescence.

The following recommendations for future work are made as a result of this investigation.

1. The experiments suggest that surface was playing an important role in absorption and desorption of hydrogen. The experiments indicate the effect of cathodic charged hydrogen on Al/SiC and Al-6061-T6 as a surface phenomenon. It is imperative to characterize and standardize the nature of the surface. The surface can be standardized by removal of the oxide layer by sputtering or by electrochemical techniques. The surface can be modified systematically and the effect of surface modification on the behavior of the material to cathodic charged hydrogen can be studied.

Surface analytical equipment can be used to characterize the surface.

2. High temperature methods of charging hydrogen can be tried to study the effect of temperature in hydrogen absorption in a composite material.

3. A method to homogenize the sample charged with hydrogen should be found out. This can help to understand the behavior of the interface of composite material in presence of internal hydrogen.

4. Embedded Atom model can be used to study the behavior of interface of composite material to internal hydrogen.

## BIBLIOGRAPHY

- 1 D. E. J. Talbot, "Effects of Hydrogen in Aluminum, Magnesium, Copper and their Alloys", International Metallurgical Reviews, Vol.20, 1975, p.166.
- 2 R. J. Gest and A. R. Troiano, "Stress Corrosion and Hydrogen Embrittlement in an Aluminum Alloy", Corrosion-NACE, Vol.30, No.8, 1974, p.274.
- 3 H. H. Johnson and J. P. Hirth, "Internal Hydrogen Supersaturation Produced by Dislocation Transport", Met trans., Vol.7A, 1976, p.1543.
- 4 J. K. Tein, A. W. Thompson, I. M. Bernstein and R. J. Richards, "Hydrogen Transport by Dislocations", Met. Trans., Vol.7A, 1976, p.821.
- 5 E. Hashimoto and T. Kino, "Hydrogen Diffusion in Aluminum at High Temperature", Met. Phy. Vol.13, 1983, p.115.
- 6 R. Eborall and C. E. Ransley, "The Reaction of an Aluminum -Magnesium Alloy with Water Vapor and the Adsorption of Hydrogen", Jour Inst Met., Vol 71, 1945, p.525
- 7 C. E. Ransley and H. Neufeld, "The Solubility of Hydrogen in Liquid and Solid Aluminum", Jour Inst Met., Vol 49, 1948/1949, p.599.
- 8 W. Von Eichenauer and A. Pebler, "Measurements of the Diffusion Coefficients and the Solubility of Hydrogen in Aluminum and Copper", Zeit Mett., Vol.48, 1957, p.373.
- 9 W. Von Eichenauer, K. Hattenbach and A. Pebler, "The Solubility of Hydrogen in Solid and Liquid Aluminum", Zeit Mett., Vol 52, (1961), p.682.
- 10 K. Kikuchi and R. B. McLellan, "The Solubility and Diffusivity of Hydrogen in Well-Annealed and Deformed Iron", Acta Met., Vol.31, 1983, p.961.
- 11 K. Papp and E. Kovacs-Cseteny, "Diffusion of Hydrogen in High Purity Aluminum", Scripta et., Vol.15, 1981, p.161.

- 12 T. Ishikawa and R. B. Mclellan, "The Difusivity of Hydrogen in Aluminum", *Acta Metall.*, Vol.34, 1986, p.1091.
- 13 G. Solt, M. Manninen and H. Beck, "Lattice Relaxation Around Interstitial Hydrogen in Aluminum", *Jour Phys F: Met Phys.*, Vol.13, 1983, p.1379.
- 14 Ritcher, "Nuclear and Electron Resonance Spectroscopes Applied to Materials Science", ed E. N. Kaufman and G. K. Shenoy (Newyork: North-Holland).
- 15 D. S. Larsen and J. K. Norskov, "Calculated Energies and Geometries for Hydrogen Impurities in Al and Mg", *J. Phys F: Metal Phys.*, Vol.9 No.10 1979, p.1975.
- 16 J. Vokl and G. Alefeld, "Diffusion of Hydrogen in Metals", *Applied Topics in Applied Physics : Hydrogen in Metals I*, G. Alefeld and J. Volkl, eds., Springer Verlag, Berlin, p.321.
- 17 Popovic and M. J. Scott, "Nonlinear, Self-Consistent Theory of Proton Screening in metals Applied to Hydrogen in Aluminum and Magnesium", *Phys Rev Lett.*, Vol.33, 1974, p.1164.
- 18 Manninen. M and Nieminen R. M *J. Phys. F: Met. Phys.*, Vol.9, 1979, p.1333.
- 19 Kahn L. M, Perrot. F and Rasolt. M, *Phys. Rev. B.* Vol.17, 1980, p.1592.
- 20 Perrot. F and Rasolt. M, *Phys. Rev. B.*, Vol.17, 1980, p.1592.
- 21 A. K. Zurek, H. L. Marcus, J. N. Cecil and R. Powers, "SIMS Study of Deuterium Trapping in Ion Implanted Aluminum Alloys", *Met Trans.*, Vol.11A, 1980, p.1920.
- 22 NR. Edwards and W. Von Eichenauer, "Reversible Hydrogen Trapping at Grain Boundaries in Super pure Aluminum", *Scripta Met.*, Vol.14, 1980, p.971.
- 23 D. A. Hardwick, A. W. Thompson and I. M. Bernstein, "The Effect of Copper Content and Microstructure on the Hydrogen Embrittlement of Al-6Zn-2Mg Alloys", *Met Trans.*, Vol. 14A, 1983, p.2517.
- 24 G. M. Schamans, "Hydrogen Bubbles in Embrittled Al-Zn-Mg Alloys", *Jour Mat Sci.*, Vol.13, 1978, p.27.

- 25 L. Cristoloudou and H. M. Flower, "Hydrogen Embrittlement and Trapping in Al-6% Zn-3% Mg", *Acta Met.*, Vol.28, 1980, p.481.
- 26 D. Nguyen, A. W. Thompson and I. M. Bernstein, "Microstructural Effects on Hydrogen Embrittlement in a High Purity 7075 Aluminum Alloy", *Acta Met.*, Vol.35, 1987, p.2417.
- 27 Asaoka, T. Dagbert, C. Aucouturier and J. Galland, J., *Scripta Met.*, Vol.11A, 1977, p.467.
- 28 B. J. Berkowitz, J. J. Burton, C. R. Helms and R. S. Polizzotti, "Hydrogen Dissociation Poisons and Hydrogen Embrittlement", *Scripta Meta*, Vol. 10, 1976, p.871.
- 29 N. E. Patan and O. Buck, "The Effect of Hydrogen and Temperature on the Strength and Modulus of Beta Phase Ti Alloys", *Effect of Hydrogen on Behavior of Materials*, Edt. Anthony W. Thompson and I. M. Bernstein.
- 30 B. Criqui, J. P. Fidelle and A. Clauss, "Effects of Internal and External Hydrogen on Mechanical Properties of Beta III Titanium Alloy Sheet", *Effect of Hydrogen on Behavior of Materials*, Edt. Anthony W. Thompson and I. M. Bernstein.
- 31 P. N. Adler, R. L. Schulte, E. J. Schneid, E. A. Kamykowski and F. J. Kuehne, "Stress Induced Hydrogen Redistribution in Commercial Titanium Alloys", *Met. Transc.*, Vol.11A, 1980, p.1617.
- 32 J. W. Watson, Y. Z. Shen and M. Meshi, "Effect of Cathodic Charging on the Mechanical Properties of Aluminum", *Met Trans.*, 1988.
- 33 M. Tehari, J. Albrecht, I. M. Bernstein and A. W. Thompson, "Strain Rate Effects on Hydrogen Embrittlement of 7075 Aluminum", *Scripta Met.*, Vol.13, 1979, p.871.
- 34 M. Mueller, I. M. Bernstein and A. W. Thompson, "Recovery Behavior of Hydrogen Charged 7075-T6 Aluminum", *Scripta Met.*, Vol.17, 1983, p.1039.
- 35 J. Albrecht, I. M. Bernstein and A. W. Thompson, "Evidence for Dislocation Transport of Hydrogen in Aluminum", *Met Trans.*, Vol.13A, 1982, p.811.
- 36 J. P. Hirth and G. J. Dienes, "On the Rate of Equilibration of Diffusional Traps in Solids", *Acta Met.*, Vol.30, 1982, p.2061.

- 37 G. Frankel and R. M. Latinson, "Hydrogen Transport during Deformation in Nickel: part II. Nickel Single Crystals", *Met Trans.*, Vol.17, 1986 B, p.869.
- 38 J. Albrecht, A. W. Thompson and I. M. Bernstein, "The Role of Microstructure in Hydrogen Assisted Fracture of 7075 Aluminum", *Met Trans.*, Vol.10A, p.1759.
- 39 D. A. Hardwick, M. Tehari, A. W. Thompson and I. M. Bernstein, "Hydrogen Embrittlement in a 2000-Series Aluminum Alloy", *Met Trans.*, Vol.13A, 1982, p.235.
- 40 J. Albrecht, B. J. McTiernan, I. M. Bernstein and A. W. Thompson, "Hydrogen Embrittlement in a High-Strength Aluminum Alloy", *Scripta Metal*, Vol.11, 1977, p.893.
- 41 J. P. Lucas, P. K. Liaw, J. J. Stephens and J. Nunes, "Effects of Particulate Fracture in Determining Fracture Toughness of Metal Matrix Composites", *Morris E. Fine Symposium*, TMS Publication, 1991, p.171.
- 42 Y. Flom and R. J. Arsenault, "Interfacial Bond Strength in an Aluminum Alloy 6061-SiC Composite", *Materials Science and Engineering*, Vol.77, 1986, p.191.
- 43 B. Roebick, "Fractography of a SiC Particulate Reinforced Aluminum Metal Matrix Composites", *Journal of Materials Science Letters*, Vol.6, 1987, p.1138.
- 44 R. O. Ritchie, W. L. Server and R. A. Wullart, "Critical Fracture Stress and Fracture Strain Models for the Prediction of Lower and Upper Shelf Toughness in Nuclear Pressure Vessel Steels", *Met. Trans.*, Vol.10A, 1979, p.1557.
- 45 F. A. Mc. Clintock, *Fracture, An Advanced Treatise*, H. Leibowitz, ed., Vol.3, p.47, Academic Press, NY, 1971.
- 46 A. C. Mackenzie, J. W. Hancock and D. K. Brown, *Eng. Fract. Mech.*, Vol.9, 1977, p.167.
- 47 C. Y. You, M. Dolalr, A. W. Thompson and I. M. Bernstein, "Microstructure Property Relationships and Hydrogen Effects in a Particulate-Reinforced Aluminum Composite", *Met. Trans.*, Vol.22A, 1991, p.2445.
- 48 T. Ishikawa and R. B. McLellan, "The Diffusivity of Hydrogen in Aluminum", *Acta. Metall*, Vol.34, No.6, 1986, p.1091.

49 David. L. McDanel, "Analysis of Stress-Strain, Fracture and Ductility Behavior of Aluminum Matrix Composites Containing Discontinuous Silicon Carbide Reinforcement", Met Trans., Vol.16A, 1985, p.1105

MICHIGAN STATE UNIV. LIBRARIES



31293015596061